



Contents lists available at ScienceDirect

Arabian Journal of Chemistry

journal homepage: www.ksu.edu.sa

Original article



Exploring sustainable corrosion inhibition of copper in saline environment: An examination of hydroquinazolinones via experimental and ab initio DFT simulations

Mohammed Oubahou^a, Mohamed Rbaa^b, Hassane Lgaz^{c,*}, Driss Takky^a, Youssef Naimi^a, Awad A. Alrashdi^d, Han-seung Lee^{e,*}

^a Laboratory of Physical Chemistry of Materials, Faculty of Science Ben M'Sik B.P.7955, Hassan II University of Casablanca, Casablanca, Morocco

^b Laboratory of Organic Chemistry, Catalysis and Environment, Department of Chemistry, Faculty of Sciences, Ibn Tofail University, PO Box 133, 14000 Kenitra, Morocco

^c Innovative Durable Building and Infrastructure Research Center, Center for Creative Convergence Education, Hanyang University ERICA, 55 Hanyangdaehak-ro, Sangrok-gu, Ansan-si, Gyeonggi-do 15588, South Korea

^d Chemistry Department, Umm Al-Qura University, Al-Qunfudah University College, Al Qunfudah 21962, 11, Saudi Arabia

^e Department of Architectural Engineering, Hanyang University-ERICA, 55 Hanyangdaehak-ro, San-grok-gu, Ansan-si, Gyeonggi-do 15588, South Korea

ARTICLE INFO

Keywords:

Hydroquinazolinones
Copper corrosion
Saline environment
Density functional theory simulation
Electrochemical methods

ABSTRACT

Copper's potential in various applications is constrained due to environmental degradation, particularly in high-salinity environments, representing a sustainability concern. Herein, two novel hydroquinazolinones, namely 1-((4-hydroxynaphthalen-1-yl)methyl)-2-phenyl-2,3-dihydroquinazolin-4(1H)-one (DQ-H) and 1-((4-hydroxynaphthalen-1-yl)methyl)-2-(p-tolyl)-2,3-dihydroquinazolin-4(1H)-one (DQ-CH₃), were analyzed for their ability to inhibit copper corrosion in a 3.5 % NaCl solution. The compounds, characterized by ¹H and ¹³C NMR, were evaluated via potentiodynamic polarization curves, electrochemical impedance spectroscopy, and weight loss measurements. Comprehensive analyses utilizing scanning electron microscopy, Fourier Transform Infrared, and UV-vis spectroscopy have revealed insights into the surface morphology and the interactive nature of inhibitor molecules with the copper surface. Our findings highlight the formation of a strong, sustainable inhibitor film on the copper surface due to the addition of hydroquinazolinones, thereby exhibiting an enhanced polarization resistance and decreased double-layer capacitance. Both DQ-H and DQ-CH₃ demonstrated a considerable inhibition effect, with efficiencies of 92 % and 94 % respectively, illustrating their potential for sustainable copper protection. Electrochemical impedance spectroscopy (EIS) results indicated a significant increase in polarization resistance from 605.7 (blank) to 9403 and 12861 Ω cm², after the addition of DQ-H and DQ-CH₃, respectively. Furthermore, the adsorption attributes of the compounds on the Cu(111) surface were examined using first-principles density functional theory simulation, revealing several covalent bonds formation. Our work aims to contribute to sustainability efforts in materials science by offering a corrosion-protective solution that is less harmful to the environment and more efficient in preserving copper's durability, particularly in saline environments.

1. Introduction

Corrosion is a widespread and pervasive problem that affects a wide range of industries and infrastructures, posing considerable economic and safety concerns worldwide. The detrimental effects of corrosion include structural damage and alterations in the chemical and physical properties of metals, leading to diminished mechanical strength and

premature failure (Khalaf et al., 2020; Sun et al., 2021; Tantawy et al., 2021; White et al., 2020). Among the metals utilized in numerous applications, copper stands out for its widespread use in critical sectors such as petrochemical, marine engineering, shipbuilding, and chemical industry (Mousavi and Baghgoji, 2016; Xia et al., 2019). Despite its exceptional electrical and thermal conductivity, as well as moderate strength, copper is susceptible to corrosion, particularly in aggressive

* Corresponding authors.

E-mail addresses: hlgaz@hanyang.ac.kr (H. Lgaz), erleehs@hanyang.ac.kr (H.-s. Lee).

<https://doi.org/10.1016/j.arabjc.2024.105716>

Received 17 August 2023; Accepted 6 March 2024

Available online 8 March 2024

1878-5352/© 2024 The Author(s). Published by Elsevier B.V. on behalf of King Saud University. This is an open access article under the CC BY-NC-ND license (<http://creativecommons.org/licenses/by-nc-nd/4.0/>).

environments containing substances like HNO_3 , H_2SO_4 , HCl , and NaCl (Aabid et al., 2021; He et al., 2020). Addressing the imperative need to prolong the service life of copper and its alloys while averting premature deterioration, the utilization of corrosion inhibitors has emerged as a prominent strategy (Al Jahdaly et al., 2022; Medupin et al., 2023; Thomas et al., 2021; Wei et al., 2020). In recent literature, the focus has been on the synthesis of a new generation of organic corrosion inhibitors that are proving remarkably effective in preventing metal corrosion. These inhibitors, particularly those containing elements such as oxygen, nitrogen, sulfur and conjugated aromatic systems, have attracted attention for their powerful corrosion control capabilities (Chaoui et al., 2020b; Shaw et al., 2019; Tan et al., 2023a). Numerous relevant and up-to-date references highlight the synthesis and performance of these innovative inhibitors, demonstrating their potential to effectively combat corrosion (Benbouguerra et al., 2018; Bourzami et al., 2019; Chafai et al., 2017, 2019; Djenane et al., 2019; Mammeri et al., 2021; Moumeni et al., 2020; Ouksel et al., 2020). Among them, the nitrogen-based heterocyclic compounds are widely used to mitigate corrosion in aqueous environments. Basically, these N-heterocyclic compounds adhere to metal surfaces using the non-bonding electrons of nitrogen and the π electrons of their side chains or aromatic rings, thus forming a protective film against corrosion (Galai et al., 2021; Gao et al., 2020). Quinazolinones, a type of N-heterocyclic compound, are easy to synthesize and boast excellent corrosion inhibiting properties as well as remarkable biological activities (Khan et al., 2014). In the field of pharmaceuticals, quinazolinones are essential building blocks for over 150 natural alkaloids derived from various plants, micro-organisms and animals. The reactivity, stability and flexibility of these compounds have made them essential intermediates in organic chemistry, facilitating their integration into medicinal applications (Alsibae et al., 2023). These applications cover a wide range of anti-inflammatory, antidepressant, anticancer, anti-allergy, hypotensive, anticonvulsant, and antimicrobial functions (Giri et al., 2009; Jafari et al., 2016; Patel et al., 2013; Reddy and Sivaramakrishna, 2020). On the other side, the corrosion-inhibiting potential of quinazolinones has been recognized, playing a role in protecting metals and extending the service life of engineered materials. For example, in a study by Zhang et al. (Zhang et al., 2016), 2-(quinolin-2-yl)quinazolin-4(3H)-one was investigated as corrosion inhibitor for Q235 steel in 1 mol/L HCl solution by means of electrochemical impedance spectroscopy (EIS), potentiodynamic polarization curves, scanning electron microscopy (SEM)/energy dispersive X-ray spectroscopy (EDX), Fourier-transform infrared (FTIR) spectroscopy and X-ray photoelectron spectroscopy (XPS) methods. The obtained results demonstrate a remarkable performance of the investigated product in terms of corrosion inhibition as it reached 91 % at 0.185 mmol/L. In another study (Ayati et al., 2011), the inhibitive effect of synthesized 2-(3-pyridyl)-3,4-dihydro-4-quinazolinone (PDQ) as a new corrosion inhibitor for mild steel in HCl (0.1 M) solution was tested employing electrochemical and thermodynamic assessments. The test data show that PDQ efficiently protects steel from corrosion by adsorption on its surface covering its active sites. Further, Aldana-González and co-workers (Aldana-gonzález et al., 2020) provided an in-depth discussion of the corrosion protection offered by a quinazoline derivative, specifically 2-bromo-6(2',6'-dichlorophenyl)dihydrobenzo [4,5]imidazo[1,2-c]quinazoline, for API 5L X52 steel in an HCl medium. Their study revealed that the inhibitor studied effectively prevented steel degradation by adsorbing onto its surface, according to the Langmuir adsorption isotherm model. Given the previous successful applications of quinazolinone derivatives developed in our laboratory for corrosion protection of steel in acidic medium (Galai et al., 2021; Oubaaqa et al., 2021; Rbaa et al., 2018; Rbaa et al., 2019a), it is worthwhile to examine the performance of this class of organic compounds for copper corrosion in chloride environments. While experimental evaluations provide crucial insights into the corrosion inhibition performance of organic compounds, theoretical approaches offer complementary perspectives by elucidating molecular-level interactions

between inhibitors and metal surfaces. Experimental evaluation of the corrosion inhibition performance of organic compounds is so far the first approach that provides a clear answer whether a given organic material is an excellent corrosion inhibitor or not. Weight loss experiments, for instance, are essential to estimate the variation of corrosion rate of metals in a corrosive medium and after adding corrosion inhibitors. A deeper insight into the corrosion inhibition mechanism and mode of action of inhibitors can be obtained from electrochemical measurements (Ahmad, 2006; Tait, 2018). Besides, surface analytical methods are used to characterize the morphology and chemical states of metal surfaces, providing evidence of the influence of inhibitors on the anti-corrosion ability of metals (Ahmad, 2006; Umoren et al., 2022). However, it is still very challenging to characterize the corrosion inhibition process due to its complexity and the influence of several factors on its performance. This can be overcome to some extent by implementing theoretical tools to assess the nature of interactions between organic compounds and metal surface, thus providing molecular-level physical insights that would explain structure/property relationships and binding mechanisms. Using computational techniques like DFT, researchers are seeking to elucidate the relationship between the molecular structure of these compounds and their inhibition efficacy. One of the main objectives is to determine the electronic properties crucial to the inhibitory action of organic compounds (Ebenso et al., 2021). In addition to electronic property calculations, molecular dynamics simulations have become a powerful tool for studying the adsorption of inhibitors to metal surfaces at the molecular level. These simulations provide detailed information on the adsorption mode of inhibitor molecules and facilitate the determination of the adsorption energy between the organic inhibitor and the metal surface (Verma et al., 2018a). However, several works have been published on the applications, advantages, and limitations of these methods in corrosion inhibition studies (Ebenso et al., 2021; Obot et al., 2019). Recent studies on the application of these theoretical models have demonstrated that their limitations are greater than their advantages (Kokalj, 2021, 2022). First-principles (*ab initio*) density functional theory (DFT) simulations are one of the most promising alternatives that can ease the understanding of complex interactions between organic molecules and metal surfaces (Kokalj, 2021, 2022). It allows the characterization of adsorption geometries, bond formation and breaking upon adsorption, and changes in chemical states before and after adsorption on the metal surface (Ebenso et al., 2021; Lgaz and Lee, 2022).

Given the abovementioned facts, this study reports the synthesis of two 8-hydroxyquinoline based quinazolinone namely, 1-((4-hydroxynaphthalen-1-yl)methyl)-2-phenyl-2,3-dihydroquinazolin-4(1H)-one (DQ-H) and 1-((4-hydroxynaphthalen-1-yl)methyl)-2-(p-tolyl)-2,3-dihydroquinazolin-4(1H)-one (DQ-CH₃) to explore their corrosion inhibition performance, adsorption characteristics and structure-activity relationship for copper in 3.5 % NaCl solution using potentiodynamic polarization curves (PPC), electrochemical impedance spectroscopy (EIS) and weight loss (WL) measurements. The nature of interactions and surface morphology of copper were experimentally evaluated using scanning electron microscope (SEM), FT-IR spectrometer, and UviLine spectrophotometer methods. Besides, a comprehensive theoretical calculation was carried out to investigate the interaction and binding mechanisms of tested compounds on the copper surface. To this end, quantum chemical parameters, first-principles DFT simulations of inhibitor adsorption geometries, and projected density of states were reported and discussed.

2. Experimental and technical details

2.1. Synthesis of hydroquinazolinones

General procedure: These organic compounds were synthesized by the reaction of 8-hydroxyquinoline with quinazolinone derivatives. In the first, we dissolved two moles of 5-chloromethyl-8-hydroxyquinoline (5-

CMHq) in a polar solvent tetrahydrofuran (THF) for a few minutes (25 min) in one mole of a weak base (NaHCO₃), after which two moles of quinazolinone derivatives (P1, P4) are added under stirring (50 °C). The reaction was brought to reflux for 12 h (Scheme 1). All chemicals were purchased from Sigma Aldrich.

1-((4-hydroxynaphthalen-1-yl)methyl)-2-(p-tolyl)-2,3-dihydroquinazolin-4(1H)-one (P1 = DQ-CH₃): Chemical Formula: C₂₆H₂₂N₂O₂, molecular Weight: 394.47.

1-((4-hydroxynaphthalen-1-yl)methyl)-2-phenyl-2,3-dihydroquinazolin-4(1H)-one (P2 = DQ-H): Chemical Formula: C₂₅H₂₀N₂O₂.

Molecular Weight: 380.44.

Spectra ¹³C and ¹H NMR for synthesized compounds are reported in the [supplementary material](#).

2.2. Materials and solutions

In this work, copper (99.9 % purity) was used to investigate the inhibition performance of the studied inhibitors. The metal was cut into small-sized rectangular coupons of dimensions 2 × 2 × 0.2 cm³ for gravimetric studies, while a cylindrical rod (8 mm diameter) of the same metal was used for electrochemical tests. The rod was covered with Teflon to only leave a surface area of 0.5 cm² in contact with the solution. Before and after each experimental manipulation, the coupons were abraded with emery paper of graded grit from 600 to 2000 degrees successively, washed with deionized water then degreased with acetone, and finally dried with hot air.

The corrosive medium of 3.5 wt% NaCl was prepared using analytical grade sodium chloride dissolved in bi-distilled water. Given the structural characteristics of DQ-H and DQ-CH₃, their appreciable solubility in a sodium chloride solution is unlikely. We therefore chose to dissolve them first in dimethylformamide (DMF), then introduce them into the test electrolyte. The concentration range of the tested products varied from 10⁻⁶ mol/L to 10⁻³ mol/L.

2.3. Electrochemical tests

The electrochemical behavior of copper in sodium chloride has been investigated with potentiodynamic polarization and electrochemical impedance spectroscopy tests. For this purpose, an assembly of the three-electrode cell was used to carry out the electrochemical experiments with a saturated calomel electrode (SCE) as a reference electrode, a platinum plate as a counter electrode, and the working electrode was a copper rod placed near the reference electrode. These tests were performed using a potentiostat/galvanostat/ PGZ100 controlled with analytics software (Voltmaster 4). The copper electrode was plunged in the examined solution for 40 min to reach the steady state open circuit potential (*E*_{OCP}) at the temperature of 298 K. PPC measurements were recorded with a scan rate of 1 mV/s in the range from -600 to 600 mV of the corrosion potential. This wide range of potentials was chosen to provide a comprehensive investigation into the influence of inhibitory

species on the observed phenomena, with a particular focus on diffusion-controlled copper dissolution.

Impedance spectra were conducted in the frequency range 100 kHz – 10 mHz by applying a sinusoidal voltage with 10 mV amplitude (peak to peak).

2.4. Weight loss method

The weight loss measurements were conducted under the approved method “ASTM G 31-72” (Abbasov et al., 2013; Verma et al., 2019). The copper sheets were mechanically polished, cleaned, dried, and carefully weighed before immersion into the corrosive medium. The specimens were kept in 50 mL of 3.5 % NaCl with and without DQ-H and DQ-CH₃ for 10 days at 298 K. Thereafter, the samples were removed from the solution, rinsed with distilled water, degreased in acetone, dried, and then reweighed. Experiments were carried out in triplicate and average results were reported. Following equations (1 and 2) were used to calculate the corrosion rate *W*_{corr} and the inhibition efficiency *IE* (%) respectively:

$$W_{\text{corr}} = \frac{\Delta m}{St} \quad (1)$$

$$IE(\%) = \frac{W_0 - W_{\text{inh}}}{W_0} \times 100 \quad (2)$$

Where *W*₀ and *W*_{inh} signified, respectively, the corrosion rate of copper in 3.5 % NaCl in the absence and presence of the inhibitor. The Δ*m* is the typical mass loss expressed in g, *S* represents the exposed area in cm², and *t* is the required immersion time of the specimens inside the corrosive solution.

2.5. Solutions and surface morphology characterization

The morphology of the copper surface was investigated by scanning electron microscopy (SEM) instrument (Hirox SH4000M) after immersion for 72 h in free and inhibited solutions at 298 K. In addition, an FT-IR spectrometer was used to evaluate the probable protective film formed on the metal surface while an analytics UVILINE spectrophotometer was used to characterize the interactions between hydroquinazolinone derivatives and Cu⁺.

2.6. Computational studies

2.6.1. Quantum chemical calculations

Full geometry optimizations of tested compounds were carried out using the density functional theory (DFT), GGA functional and DNP basis set (Grimme, 2006) along with COSMO solvation model using DMol3 code (Delley, 2000, 1990). Computed quantum chemical parameters include the energy of the highest occupied molecular orbital (*E*_{HOMO}), the energy of the lowest unoccupied molecular orbital (*E*_{LUMO}), energy band gap (Δ*E*_g), and the fraction of transferred electrons (Δ*N*) among others. These quantum chemical reactivity indices are calculated via the following relationships as previously reported in literature (Ansari et al., 2022):

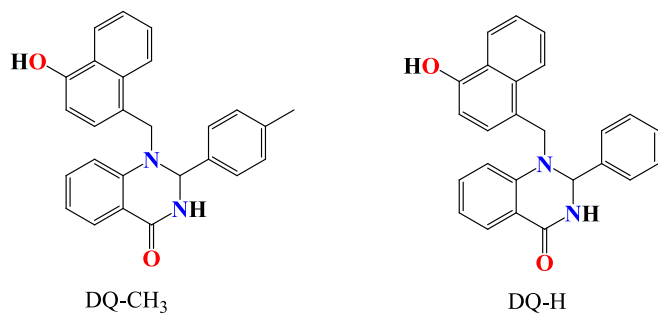
$$\Delta E = E_{\text{LUMO}} - E_{\text{HOMO}} \quad (3)$$

$$IE = -E_{\text{HOMO}} \quad (4)$$

$$EA = -E_{\text{LUMO}} \quad (5)$$

$$\eta = \frac{IE - EA}{2} \quad (6)$$

$$\sigma = \frac{1}{\eta} \quad (7)$$



Scheme 1. Molecular structures of investigated quinazolinone derivatives DQ-CH₃ and DQ-H.

$$\chi = \frac{IE + EA}{2} \quad (8)$$

$$\mu = \frac{-(IE + EA)}{2} \quad (9)$$

Fukui function indices were analyzed according to Hirshfeld population analysis using the following equations (Fukui, 1982):

$$f_k^+ = q_k(N+1) - q_k(N) \quad (10)$$

$$f_k^- = q_k(N) - q_k(N-1) \quad (11)$$

where, $q_k(N+1)$, $q_k(N)$, and $q_k(N-1)$ are the electron densities on atom k corresponding to $N+1$, N and $N-1$ electrons systems, respectively.

2.6.2. First-principles DFT simulations

Inhibitor-iron interactions were fully optimized by spin polarized first-principles DFT, including dispersion interaction (DFT-D3) and ultra-soft pseudopotentials using the CASTEP code (Clark et al., 2005). The generalized gradient approximation (GGA) within its PBE formulation was used for the electron exchange and correlation (Perdew et al., 1996). The adsorption systems were fully optimized using a self-consistent field (SCF) tolerance of 10^{-6} eV/atom, and plane-wave basis set with an energy cut-off of 30 Ry. All other convergence tolerance values were set according to fine quality. Meanwhile, the bulk lattice parameters optimization was carried out using (8x8x8) k-point grid, which was reduced to (2x2x1) k-point grid for adsorption models. Inhibitor-iron adsorption models were generated by constructing Cu (111) copper surface consisting of a (5x5) supercell and a vacuum spacing of 20 Å along the z-direction separating periodic image in each direction. Then, inhibitor molecules were placed on the top side of the slab and all atoms were allowed to relax except the two bottom-most atomic layers. Optimization of standalone molecules was conducted on a cubic box of 30 Å in size. Origin 2016 and Inkscape software were used for plotting and post-processing of all figures. The total energies of isolated molecules (noted E_{mol}), Cu(111) copper surface (noted E_{surf}), and molecules/Cu(111) adsorption systems (noted $E_{mol/surf}$) were used to determine the adsorption binding energy as:

$$E_{inter} = E_{mol/surf} - (E_{mol} + E_{surf}) \quad (12)$$

The selection of the high-density Cu (111) surface model for the study of DQ-H, DQ-CH₃ adsorption is based on its characteristics as the most stable surface among low-Miller index copper surfaces and on its predominance. This dual attribute underlines its relevance as a representative model for the study of these compounds (Sun et al., 2012; Vitos et al., 1998).

3. Results and discussion

3.1. Weight loss measurements

The experimental data derived from weight loss measurements for copper in 3.5 % NaCl medium without and with various doses of DQ-H and DQ-CH₃ are represented in Fig. 1 and Table 1.

Gravimetric analysis results indicate a significant decrease in corrosion rate with increasing compound concentrations in the 3.5 % NaCl solution, demonstrating the inhibitors' effectiveness in mitigating copper corrosion. Besides, high inhibition efficiencies were observed at all concentrations for DQ-H and DQ-CH₃. Notably, at a concentration of 10^{-3} mol/L, DQ-H and DQ-CH₃ showed remarkable inhibition efficiencies of 93.85 % and 93.25 %, respectively, underlining the strong inhibitory properties of hydroquinazolinones under these experimental conditions. These high inhibition levels result mainly from the adsorption of inhibitor molecules onto the metal surface, which reduces metal

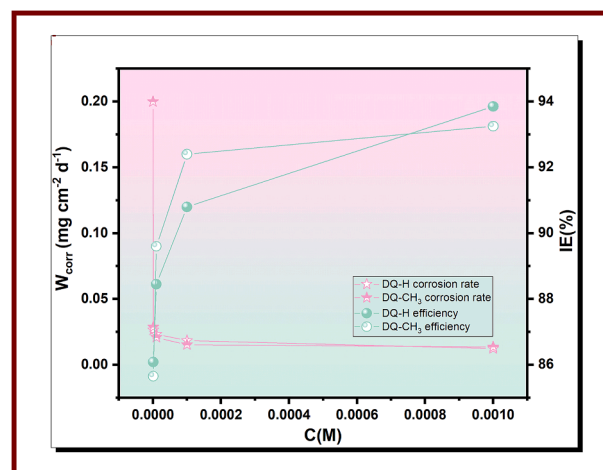


Fig. 1. Weight loss results of copper in 3.5 % NaCl with and without various concentrations of DQ-H and DQ-CH₃ at 298 K.

Table 1

Corrosion rates and inhibition efficiencies of various concentrations of the tested compounds in 3.5 % NaCl at 298 K.

Inhibitor	Concentration(mol/L)	W_{corr} (mg cm ⁻² d ⁻¹) × 10 ⁻²	Surface coverage (θ)	IE(%)
Blank	–	20	–	–
	10 ⁻⁶	2.64	0.8608	86.08
	10 ⁻⁵	2.31	0.8845	88.45
	10 ⁻⁴	1.84	0.9080	90.80
	10 ⁻³	1.23	0.9385	93.85
	10 ⁻⁶	2.87	0.8585	85.85
	10 ⁻⁵	2.08	0.8960	89.60
3	10 ⁻⁴	1.52	0.9240	92.40
	10 ⁻³	1.35	0.9325	93.25

dissolution by blocking the active sites (Zhang et al., 2018b). From a mechanistic perspective, these compounds have the ability to form coordination complexes with copper in its various oxidation states (0, I, II). The possibility of forming chelated complexes arises when these molecules engage in donor-acceptor interactions, in which the free electron pairs of the heteroatoms (O, N) interact with the vacant d-orbitals of copper. (Otmacic Curkovic et al., 2010). Generally, the corrosion-inhibiting attributes of these molecules derive from their structural features, in particular the presence of lone and π electrons, crucial for their adsorption to the target metal surface. Changes in the chemical structure of organic molecules, including variations in heteroatoms, functional groups, phenyl rings, their positions and natures, significantly influence the adsorption strength and stability of the adsorbed film (Ouici et al., 2015; Tan et al., 2023b). The following sections of this research will look at relevant cases illustrating these phenomena.

3.2. Electrochemical impedance spectroscopy studies

EIS, known for its effectiveness in revealing precise aspects of corrosion mechanisms, was used in this study (Sukul et al., 2018). The impedance plots of copper in 3.5 % NaCl without and with different concentrations of DQ-H and DQ-CH₃ were carried out automatically after a stabilization period of 2400 s at 298 K and shown in Fig. 2. The Bode diagrams shown in Fig. 2 (a) and (b) reveal a significant increase in impedance values over the entire frequency spectrum with increasing DQ-H and DQ-CH₃ concentration. Also, analysis of the Bode phase diagrams reveals the presence of two relaxation time constants governing the corrosion process occurring at the electrode surface. One is linked to the relaxation of the electric double-layer capacitor, while the other is

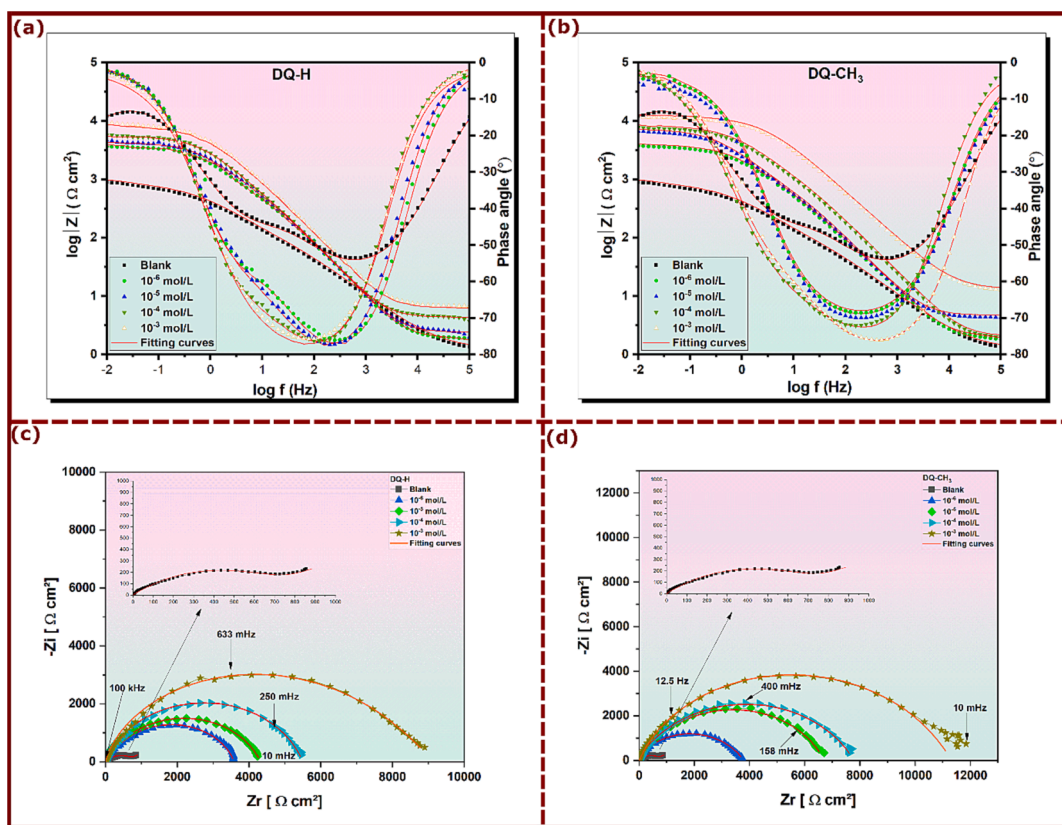


Fig. 2. Bode and Nyquist plots for copper in 3.5% NaCl with and without DQ-H and DQ-CH₃ concentrations; (a)-(b) Bode, and (c)-(d) Nyquist plots.

associated with the relaxation process of the adsorbed inhibitors (Sherif et al., 2008). Furthermore, it can be seen that an increase in quinazolines' concentration leads to a corresponding increase in the maximum phase angle shown in Fig. 2 (a) and (b), indicating an inhibition action of the corrosion process (Hong et al., 2012).

In the presence of quinazolines, the impedance spectra for the Nyquist plots (Fig. 2 (c) and (d)) clearly show a depressed semicircle in the high frequency region. This depressed semicircle is attributed to the charge transfer and double-layer capacitance (Deslouis et al., 1988; Hong et al., 2012; Tribollet, 1994). While in the absence of DQ-H and DQ-CH₃, the depressed semicircle of Nyquist plot is followed by a straight line at low frequency region. Generally, the presence of a diffusion layer around the electrode surface, characterized by an ion concentration gradient due to electrochemical reactions, is a common phenomenon when an electrode is immersed in an ion-containing solution. More specifically, in the case of copper dissolution in NaCl solution, the appearance of a Warburg line on the blank Nyquist diagram indicates that the copper dissolution process is mainly controlled by diffusion. This suggests that the rate of copper dissolution is limited by the transport of copper ions through the diffusion layer around the electrode (Chen et al., 2018; Liao et al., 2011; Yao et al., 2021). In the present circumstances, one may suggest that copper undergoes various electrochemical reactions, leading to the formation of complexes such as CuCl and CuCl₂. At the interface between the copper electrode and the solution, adsorption of ions from the solution onto the electrode surface results in the formation of an electrical double layer. This later functions as a capacitor, capable of storing charges and thus influencing the impedance of the system (Sukul et al., 2018). It is also clear from Fig. 2 (b) and (c) that the diameter of the Nyquist semicircle grows with increasing concentration of the inhibitors accompanied with a complete disappearance of Warburg line. The absence of Warburg line in the Nyquist plots of the inhibited solutions implies that the DQ-H and DQ-CH₃ have attenuated the electrochemical reactions associated with mass

transfer, indicating protective ability of quinazolines by adsorption on the copper surface covering its active sites (Dafali et al., 2003; Sukul et al., 2018).

The impedance characteristics were analyzed using the equivalent circuit models shown in Fig. 3. This circuit models were also reported in various studies for Cu/NaCl system (Hong et al., 2012).

The parameters determined by fitting the equivalent circuits, along with the calculated inhibition efficiencies, are presented in Table 2. Here, R_s represents the resistance of the studied medium, R_f is the

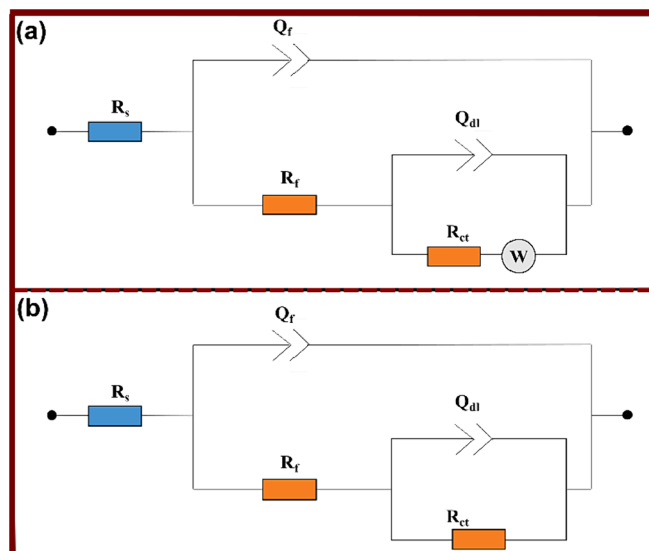


Fig. 3. Equivalent circuits models that have been used to fit EIS data of un-inhibited (a) and inhibited (b) solutions.

Table 2EIS parameters of copper corrosion in the absence and presence of DQ-H and DQ-CH₃ in 3.5 % NaCl at 298 K.

Inhibitor	Conc (mol/L)	$R_s(\Omega.cm^2)$	$C_f(\mu F.cm^2)$	n_1	$R_f(\Omega.cm^2)$	$C_{dl}(\mu F.cm^2)$	n_2	$R_{ct}(\Omega.cm^2)$	$R_p(\Omega.cm^2)$	$W(\Omega.cm^2)$	$\chi^2 \times 10^{-3}$	$\eta_{EIS}(\%)$
Blank	–	1.019	54.3	0.6907	144.6	174.66	0.6504	605.7	750.3	49.15	0.690	–
	10^{-6}	1.876	23.02	0.9178	570	48.57	0.7527	3020	3590	–	0.302	79.10
	10^{-5}	2.404	23.00	0.9227	795	43.21	0.7095	3529	4324	–	0.319	82.65
	10^{-4}	4.353	22.86	0.9242	1011	23.66	0.7062	4493	5504	–	0.264	86.37
	10^{-3}	6.696	16.00	0.9029	1464	9.1	0.4878	7939	9403	–	6.359	92.02
DQ-CH ₃	10^{-6}	1.831	21.79	0.8699	508.1	28.57	0.5789	3303	3811	–	0.181	80.31
	10^{-5}	4.292	20.77	0.8960	862	26.19	0.7097	5842	6704	–	0.379	88.80
	10^{-4}	1.863	10.64	0.8898	1320	20.13	0.6465	6479	7799	–	6.793	90.38
	10^{-3}	2.979	4.13	0.9138	1454	18.22	0.6765	11,407	12,861	–	0.380	94.17

resistance of the formed film on the copper surface, Q_f and Q_{dl} refer to constant phase elements (CPE), R_{ct} is the charge transfer resistance, and W signifies the Warburg element (Kannan et al., 2018). According to the roughness of the electrode surface and frequency dispersion, the capacitive loops of Nyquist diagrams were not perfectly semicircular. As a result, the use of CPE instead of pure capacitance is more suitable to fit the obtained EIS data. The double-layer capacitance C_{dl} and film capacitance C_f were determined by equations 13 and 14 respectively (Tasić et al., 2021):

$$C_f = (Q_f R_f^{1-n_1})^{1/n_1} \quad (13)$$

$$C_{dl} = (Q_{dl} R_{dl}^{1-n_2})^{1/n_2} \quad (14)$$

Table 2 clearly shows that CPE values decrease as quinazolinones' concentration increases. This trend is expected to cover the charged surface, thus reducing the capacitive effect. The decrease in C_{dl} with increasing DQ-H and DQ-CH₃ concentration can be attributed to the formation of a double layer between the charged metal surface and the solution, which functions as an electrical capacitor (Tan et al., 2022a, Tan et al., 2022b). Adsorption of inhibitor molecules at the metal/solution interface can lead to a decrease in the local dielectric constant and/or an increase in the thickness of the electrical double layer (Ashassi-Sorkhabi et al., 2005). Moreover, the values of the polarization resistance (R_p is the sum of R_f and R_{ct}) increase significantly as the concentration of both inhibitors increases, which explains the increase in the surface covered by the adsorption of inhibitor molecules (El et al., 2023; Galai et al., 2020). The inhibition effectiveness η_{EIS} (%) of DQ-H and DQ-CH₃ is described as follows:

$$\eta_{EIS} = \frac{R_p - R_p^0}{R_p} \times 100 \quad (15)$$

Herein R_p and R_p^0 are polarization resistances in solutions with and without DQ-H and DQ-CH₃, respectively.

The Inhibition efficiencies, derived from R_p , show an upward trend with increasing inhibitor concentration. The highest value recorded was 92.02 % for DQ-H and 94.17 % for DQ-CH₃ at 10^{-3} mol/L. The strong inhibitory capacity of these inhibitors is attributed to their association with high electron density, particularly notable in the π electrons of aromatic rings, as well as in the non-bonding electrons of oxygen and nitrogen atoms (Verma et al., 2020).

The introduction of an additional methyl group into the molecular structure of quinazolinones appears to have a slight effect on their inhibition efficacy against copper corrosion in NaCl solution. The observed inhibition efficiencies of 94.17 % for DQ-CH₃ and 92.02 % for DQ-H underline the impact of structural modifications on corrosion inhibition properties. Although the improvement in inhibition efficiency with the addition of a methyl group may not be significant, it could be attributed to several factors. Firstly, the presence of the methyl group may lead to changes in the electronic structure of the molecule, influencing its interaction with the metal surface and facilitating stronger adsorption to the copper substrate. In addition, steric effects introduced

by the methyl group could alter the spatial arrangement of inhibitor molecules at the metal/solution interface, potentially enhancing their coverage and effectiveness in corrosion inhibition (Verma et al., 2018). Similar trends have been observed in recently published studies on the effect of structural modifications on corrosion inhibition performance. For example, a study by El-Haddad et al. (El-Haddad and Fouda, 2015) investigated the corrosion inhibition efficacy of imidazole derivatives, both with and without alkyl groups, on aluminum in a 0.5 M HCl solution. Their findings demonstrated that methyl imidazole exhibited superior corrosion inhibition compared to regular imidazole. Interestingly, the methyl substituent did not alter the mechanism of action of imidazole; instead, it enhanced the compound's coverage and adsorption on the aluminum surface. Similarly, research by Chaouiki et al. (2020a) reported improved inhibition efficacy with the addition of methyl group to quinoxaline derivatives for mild steel corrosion inhibition in acidic medium. Specifically, 8-Hydroxyquinoline, namely 1-((8-hydroxyquinolin-5-yl)methyl)-3,6-dimethylquinoxalin-2(1H)-one (Q1) achieved an efficacy of 96 %, whereas 1-((8-hydroxyquinolin-5-yl)methyl)quinoxalin-2(1H)-one (Q2) reached 89 %. This phenomenon extends beyond the substitution of the methyl group. Numerous papers have also examined the impact of substituents such as $-OCH_3$, $-NH_2$, $-OH$ and others on the inhibition efficacy of organic N-heterocyclic inhibitors. Gad Allah et al. (Gad Allah et al., 1989) outlined the corrosion inhibition properties of various pyrazole derivatives on zinc corrosion in hydrochloric acid solution through capacitance and polarization measurements. Their findings revealed the following order of inhibition efficiencies attributed to different substituents within the molecules: $-H$ (77 %) < $-CH_3$ (85 %) < $-OCH_3$ (87.8 %). For mild steel corrosion in 2 M HCl solution, double Schiff base derivative with $-OCH_3$ and $-OH$ substituents showed better corrosion protection as compared to non-substituted one (Soltani et al., 2010). Similar observation has been reported for pyridine derivatives, where for acidic corrosion of mild steel methyl and methoxy substituents manifest better protection ability as compared to non-substituted compound (Noor and Al-Moubaraki, 2008). What these groups have in common, then, is their nature as electron-donating moieties. It has been reported that electron-donating substituents such as $-OH$, $-NH_2$, $-CH_3$ and $-OCH_3$ increase the electron density at the adsorption center of the inhibitor, thereby intensifying interactions between the inhibitor molecule and the metal surface (Belghiti et al., 2022). These results underline the importance of molecular design and structural optimization in tailoring the corrosion inhibition properties of organic compounds, with the addition of methyl groups a promising strategy for enhancing their effectiveness in protecting metals against corrosion in chloride-containing environments. But what about other groups of the opposite nature, i.e. electron-attracting substituents?

3.3. Potentiodynamic polarization measurements

The cathodic and anodic polarization curves of copper in 3.5 % NaCl solution at 298 K were analyzed in the absence and presence of varying concentrations of DQ-CH₃ and DQ-H, as shown in Fig. 4. Electrochemical parameters, including corrosion potential (E_{corr}), corrosion

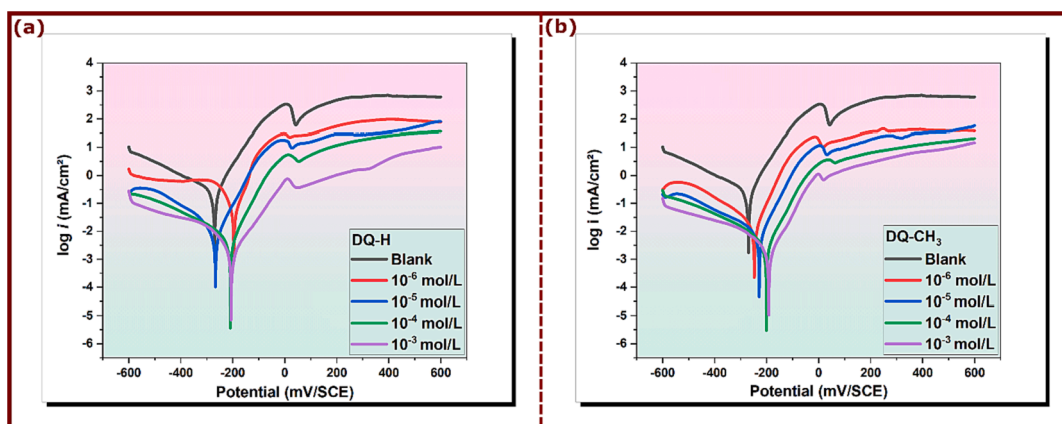


Fig. 4. PP curves of copper/3.5 % NaCl in the presence and absence of DQ-H (a) and DQ-CH₃ (b) at 298 K.

current density (i_{corr}), cathodic and anodic Tafel constants (β_c and β_a), shown in Table 3, were obtained by extrapolating current–potential (i - E) curves. Inhibition efficiency was calculated using equation (21), where i_{corr} and i_{inh} are the corrosion current density values without and with DQ-CH₃ and DQ-H, respectively (Abd El-Lateef et al., 2020, 2022).

$$\eta_{PDP} = \left(1 - \frac{i_{inh}}{i_{corr}}\right) \times 100 \quad (21)$$

Copper and its alloys are known for their exceptional resistance to corrosion in saline environments (Chauhan et al., 2019; Finšgar and Milošev, 2010). It is proposed that the dissolution of copper in a chloride medium occurs in several steps. The initial step involves the oxidation of Cu(0) to Cu(I) (eq. 22), which leads to a rise in current density from anodic potentials to a peak value (i_{max}).



Subsequently, current density decreases due to the formation of an insoluble CuCl film facilitated by the presence of Cl⁻ ions (Eq.23). As CuCl is unstable, it then reacts with Cl⁻ ions to form the soluble compound CuCl₂⁻ (Eq.24), resulting in a further increase in current density from i_{max} to a minimum value (i_{min}) (W. Li et al., 2011).



Once adsorbed on the surface, the cuprous chloride (CuCl₂⁻) complex undergoes further oxidation, as described in equation 25:



The cathodic corrosion reaction in NaCl solution should be the reduction of oxygen:



In addition, these reactions are followed by the formation of copper oxide Cu₂O (Eq.27) (El-Hajjaji et al., 2020).

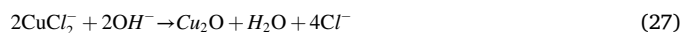


Fig. 4a and 4b show that the inclusion of quinazolinone derivatives reduces both cathodic and anodic currents, preventing chloride attack on the copper electrode in 3.5 % NaCl. Generally, adsorption of inhibitors can significantly influence corrosion rates through two main mechanisms. Firstly, inhibitors can reduce the available reaction zone, a phenomenon known as the geometric blocking effect. This reduction limits the access of corrosive agents to the metal surface, preventing the initiation and propagation of corrosion. Secondly, inhibitors can modify the activation energy required for cathodic and anodic reactions, thus affecting the kinetics of the corrosion process (M. E. Belghiti et al., 2016). It has been discussed that in the case of the first mode, inhibition arises from the reduction of the reaction zone on the surface of the corroded metal, whereas for the other two modes, inhibition effects arise from changes in the average activation energy barriers of the anodic and cathodic reactions of the corrosion process (Muralidharan et al., 1995). The values of the cathodic Tafel slope (β_c) shows slight changes when DQ-H and DQ-CH₃ are added, indicating that the inhibitory action occurs by simply blocking the available cathodic sites on the metal surface. Furthermore, the values of the anodic Tafel slopes (β_a) also change with the addition of DQ-H and DQ-CH₃, suggesting that these inhibitors are initially adsorbed onto the metal surface and hinder by simply blocking the reaction sites on the metal surface without affecting the mechanism of the anodic reaction (Ouakki et al., 2020). Moreover, the displacement in E_{corr} value was less than 85 mV between blank, and inhibited solution. On the basis of these results, the DQ-H and DQ-CH₃ derivatives can be classified as mixed-type inhibitors in 3.5 % NaCl, delaying both anodic and cathodic corrosion reactions with a predominant effect on the anodic reaction (Abdelsattar et al., 2020; Belhadi et al., 2023). Table 3 also shows that current density undergoes a noticeable decrease with increasing DQ-H and DQ-CH₃ concentration. In the absence of

Table 3

Polarization data and the corresponding inhibition efficiencies of copper in 3.5 % NaCl with and without various concentrations of DQ-H and DQ-CH₃ at 298 K.

Medium	Concentration(mol/L)	$-E_{corr}$ (mV vs. SCE)	β_a (mV dec ⁻¹)	$-\beta_c$ (mV dec ⁻¹)	i_{corr} ($\mu\text{A cm}^{-2}$)	η_{PDP} (%)
Blank	–	267.8	49.6	78	131.4	–
	10 ⁻⁶	194	44.7	43.9	36.8	71.99
	10 ⁻⁵	264.8	56.8	84.7	8.46	93.56
	10 ⁻⁴	207	58.5	131.2	4.04	96.65
	10 ⁻³	204.7	94.6	100.6	2.17	98.34
3	10 ⁻⁶	245.2	48.1	84.2	10.1	92.31
	10 ⁻⁵	225.7	49.8	93.3	5.11	96.11
	10 ⁻⁴	198.9	59.8	115.4	2.62	98.00
	10 ⁻³	189.8	72	100.2	1.67	98.73

inhibitors, current density is measured at $131.4 \mu\text{A}/\text{cm}^2$, while in the presence of 10^{-3} mol/L DQ-H and DQ-CH₃, it decreases significantly to $2.17 \mu\text{A}/\text{cm}^2$ and $1.67 \mu\text{A}/\text{cm}^2$, respectively. This observation indicates that the quinazolinone derivatives studied show increasing adsorption to the copper surface as their concentration increases. This adsorption leads to coverage of the active sites on the copper surface, forming a protective layer that decreases the reactivity of copper dissolution (Verma et al., 2017).

As previously indicated, the size and active centers within the molecular structure of organic compounds play a crucial role in determining their inhibitory efficacy (Huang and Guo, 2020). Consequently, the inhibition efficacy of quinazolinones, as assessed by potentiodynamic polarization measurements, aligns with the results obtained by electrochemical impedance spectroscopy (EIS) tests. Specifically, the inhibition efficiency for DQ-CH₃ is calculated at 98.73 %, which is slightly higher than the 98.34 % measured for DQ-H. The corrosion inhibition effect is attributed to the presence of several π -systems of the aromatic rings and several nitrogen atoms in the main molecular structure of both DQ-H and DQ-CH₃ that would act as adsorption centers. Functional groups would have a great influence on the corrosion inhibition performance of compounds when they are directly contributing to the binding and affinity to metal surfaces. In the present case, the core of both compounds is the main responsible for the adsorption of molecules on the copper surface and that is why the influence of the additional methyl group is negligible. It should be noted that, although the introduction of a -CH₃ group into the molecular structure does not significantly affect corrosion performance in the current scenario, some research papers in references (Bentiss et al., 2007; Isin and Karakus, 2015; Zaaferany, 2009) demonstrated that the addition of certain substituents to the molecular skeleton of an inhibitor significantly enhances its corrosion inhibition capability. In our previously published article (Oubahou et al., 2023), we studied the efficacy of three isomers, namely: 2-(4-chlorophenyl)-1-((4-hydroxynaphthalen-1-yl)methyl)-2,3-dihydroquinazolin-4(1H)-one (DQ-Cl), 2-(4-bromophenyl)-1-((4-hydroxynaphthalen-1-yl)methyl)-2,3-dihydroquinazolin-4(1H)-one (DQ-Br), and 2-(2-chlorophenyl)-1-((4-hydroxynaphthalen-1-yl)methyl)-2,3-dihydroquinazolin-4(1H)-one (DQ-Cl'), under the same experimental conditions as the current study. Comparing the results of our previous research with those of the present study, we observed that DQ-H and DQ-CH₃ showed higher inhibition efficiencies than halogenated quinazolinones. The order of efficacy is as follows: DQ-CH₃ > DQ-H > DQ-Br > DQ-Cl > DQ-Cl'. The improved performance of DQ-CH₃ and DQ-H compared with DQ-Br, DQ-Cl and DQ-Cl' can be explained by the fact that halogen substituents withdraw electrons. As established, electron-donating substituents increase the electron density at the adsorption center of the inhibitor, thus promoting its affinity for the metal surface. Conversely, electron-withdrawing substituents such as -Br, -Cl, -NO₂, -CN, -COOH, and -COOC₂H₅ decrease the electron density at the adsorption center, thus reducing the interaction between inhibitor molecules and the metal surface (Harvey et al., 2011; Li et al., 1999). Table S3 (supplementary material) compares the corrosion inhibition performance of several other quinazolinones previously used for metal corrosion protection (Ayati et al., 2011; Chen et al., 2021a; Errahmany et al., 2020; Fouda et al., 2010; Rbaa et al., 2019b; Zhang and Zhang, 2021). It is evident that DQ-H and DQ-CH₃ exhibit reasonable corrosion inhibition efficiencies compared with other quinazolinones listed in Table S3. Furthermore, the data in Table S3 underline that the nature and/or position of substituents can, in some cases, influence inhibitor efficacy (Arrousse et al., 2022; Faydy et al., 2019; Fouda and Hassan, 2013; Khan et al., 2017; Kumar et al., 2020).

3.4. Temperature effect

It is acknowledged that the temperature has a significant impact on the corrosion process resulting in a modification in the mechanism of the inhibitor's action on a metallic surface (Boudjellal et al., 2020; Damej

et al., 2021; Galai et al., 2020; Ouici et al., 2013). To study the effect of temperature on the protective power of the investigated hydroquinazolinones, potentiodynamic polarization measurements were conducted for copper in 3.5 % NaCl in the presence and absence of 10^{-3} mol/L of DQ-CH₃ and DQ-H in the temperature range of 298–328 K. The obtained curves are shown in Fig. 5. In addition, a summary of electrochemical parameters is listed in Table 4.

The rise in temperature leads to the modification of E_{corr} values in both uninhibited and inhibited solutions. At the same time, the anodic and cathodic current densities increased especially for uninhibited medium indicating that the corrosion rate of copper is influenced by the temperature (Hrimla et al., 2021). The changes observed in E_{corr} and i_{corr} coincide with a decrease in inhibitory efficiency, showing a slight decline to 86.75 % for DQ-H and 87.72 % for DQ-CH₃ at 328 K,

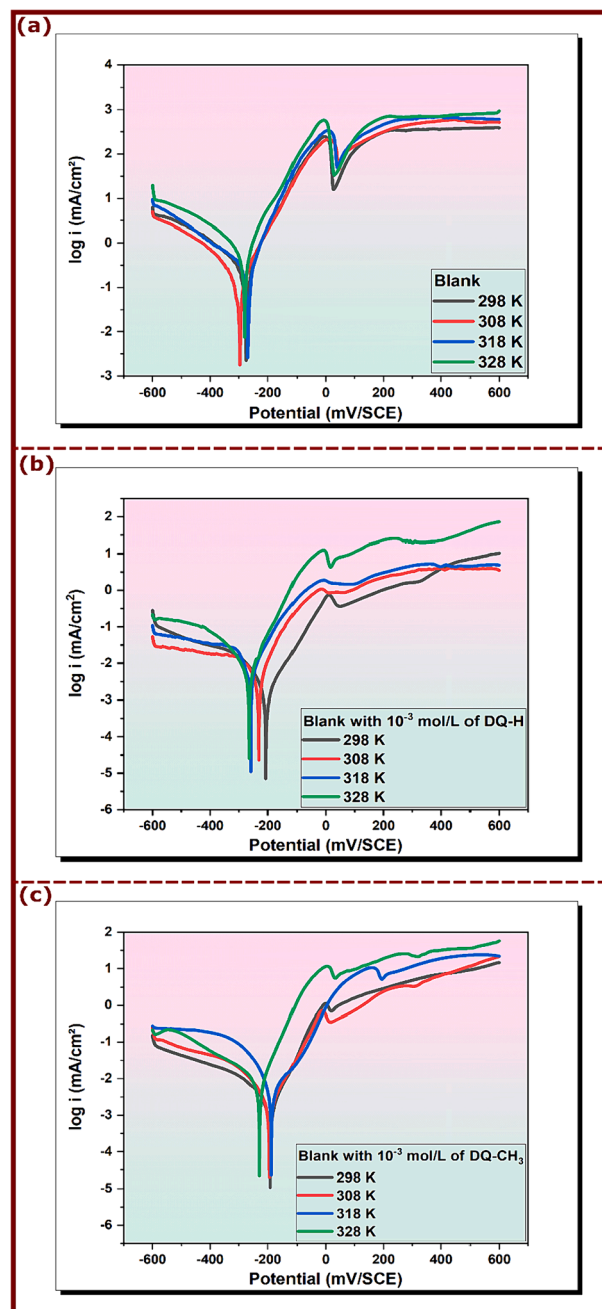


Fig. 5. Tafel plots of the copper electrode in 3.5 NaCl with and without 10^{-3} mol/L of DQ-H and DQ-CH₃ at different temperatures; (a) Blank, (b) DQ-H and (c) DQ-CH₃.

Table 4Electrochemical data of copper in 3.5 % NaCl with and without 10^{-3} mol/L of DQ-H and DQ-CH₃ at different temperatures.

Medium	Temperature(K)	$-E_{corr}$ (mV vs. SCE)	βa (mV dec ⁻¹)	$-\beta c$ (mV dec ⁻¹)	i_{corr} ($\mu A cm^{-2}$)	η_{PDP} (%)
Blank	298	267.8	49.6	78.0	131.40	–
	308	296.6	81.9	132.1	234.70	–
	318	275.1	69.7	127.0	436.0	–
	328	277.6	72.4	157.5	732.80	–
DQ-H	298	204.7	94.6	100.6	2.17	98.34
	308	228.7	54.5	104.1	11.43	95.13
	318	256.4	67.8	78.8	40.80	90.64
	328	262.5	66.8	113.2	97.10	86.75
DQ-CH ₃	298	189.8	72.0	100.2	1.67	98.73
	308	192.6	81.0	103.3	9.15	96.10
	318	185.4	124.4	78.2	48.36	88.91
	328	225.7	58.1	135.6	89.97	87.72

respectively. This trend can be attributed to the intensification of corrosion activity leading to surface roughening of copper (El Mouaden et al., 2018). More specifically, the acceleration of various corrosion processes, including electrochemical and chemical reactions, as well as the transfer of reactive species to the metal surface, is enhanced at higher temperatures (Desimone et al., 2011). Despite these difficulties, it should be noted that DQ-H and DQ-CH₃ compounds retain strong inhibition capabilities even at elevated temperatures, underscoring their effectiveness in corrosion mitigation.

For further details on the copper corrosion process, activation energy E_a for the adsorption of DQ-CH₃ and DQ-H on copper in the absence and presence of 10^{-3} mol/L is calculated using the Arrhenius equation (Eq.28) (El-Hajjaji et al., 2018).

$$i_{corr} = A e^{-\frac{E_a}{RT}} \quad (28)$$

Where A is the pre-experimental factor, R represents the universal gas constant and T refers to the absolute temperature. Fig. 6 illustrates the Arrhenius plots of the corrosion current densities versus $1/T$ for copper in the corrosive environment without and with the addition of the investigated compounds, at their maximum concentrations.

The addition of DQ-CH₃ and DQ-H to the blank solution moves significantly the E_a from being 46.93 kJ mol⁻¹ in the free solution to a higher value in the presence of inhibitors where it reaches 103.35 and 111.21 kJ mol⁻¹ for 10^{-3} mol/L of DQ-H and DQ-CH₃ respectively. Hence, there is less metal dissolution, which justifies the rise in activation energy (Rouifi et al., 2020). Also, the higher value of activation energy in the presence of DQ-H and DQ-CH₃ indicates that the inhibitor molecules adsorb on the copper surface in a strong way (Hamdy and El-Gendy, 2013).

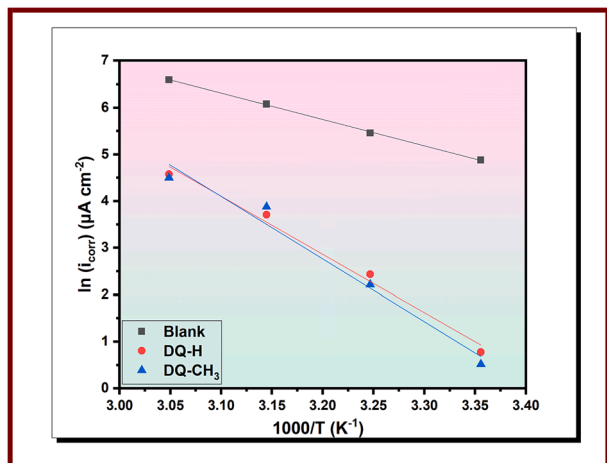


Fig. 6. Arrhenius plots for copper corrosion in 3.5 % NaCl in the absence and presence of 10^{-3} mol/L of DQ-H and DQ-CH₃.

3.5. Adsorption isotherms

Inhibitors based on organic molecules adsorb on the metal/solution interface and create protective films (Lgaz et al., 2020). To get a better understanding of the adsorption mechanism of DQ-H and DQ-CH₃ on the copper surface, it is vital to determine which form of adsorption, whether physical or chemical, has taken place during that process. For this purpose, Langmuir (Eq. 29) (El et al., 2023), Frumkin (Eq. 30) (Souza and Spinelli, 2009), Temkin (Eq. 31) (Akinbulumo et al., 2020), Freundlich (Eq. 32) (Belhadi et al., 2023), and El-Awady (Eq.33) (El-Awady et al., 1990; El-Awady et al., 1992) isotherms were used to simulate the changes in the coverage rate (θ) obtained from PPC measurements, with the concentration of the inhibitor. These models were calculated using the following equations and were plotted in Fig. 7.

$$\frac{C_{inh}}{\theta} = \frac{1}{K_{ads}} + C_{inh} \quad (29)$$

$$\log \left[\left(\frac{\theta}{(1-\theta) \times C_{inh}} \right) \right] = \log K_{ads} + g \quad (30)$$

$$\ln C_{inh} = g\theta - \ln K_{ads} \quad (31)$$

$$\log \theta = n \log C_{inh} + \log K_{ads} \quad (32)$$

$$\log \left[\left(\frac{\theta}{1-\theta} \right) \right] = y \log K_{ads} + g \log C_{inh} \quad (33)$$

Herein, C_{inh} is the inhibitor concentration, K_{ads} represents the adsorption equilibrium constant, n is the constant of Freundlich and g is the adsorbate interaction parameter.

The comparison of the correlation coefficient R^2 of the listed models shows that the Langmuir isotherm presents the highest R^2 value and thus, it is the suitable model to describe the adsorption of DQH and DQCH₃ on the copper surface (Galai et al., 2021). On the other side, high values of K_{ads} illustrated in Table 5 suggest that the inhibitors under examination interact strongly with the surface of the metal (Al-Azawi et al., 2018). The standard free energy is directly related with K_{ads} by the following equation (27) (Lgaz et al., 2017):

$$\Delta G_{ads}^0 = -RT \ln \{ (55.5 K_{ads}) \} \quad (27)$$

Where R expressed in J/mol K⁻¹ is the universal gas constant, 55.5 is the molar concentration of water (mol/L) and T is the temperature.

It has been reported that values of ΔG_{ads}^0 around -20 kJ.mol⁻¹ or less negative, characterize an electrostatic adsorption process (physisorption), whereas values around -40 kJ mol⁻¹ or more negative correspond to chemisorption (Alaoui et al., 2019; Yildiz et al., 2014; Zhang et al., 2018a). In corrosion inhibition studies, many previously published works use the fitting of isotherm models to experimental data to determine some thermodynamical parameters like ΔG_{ads} values, then

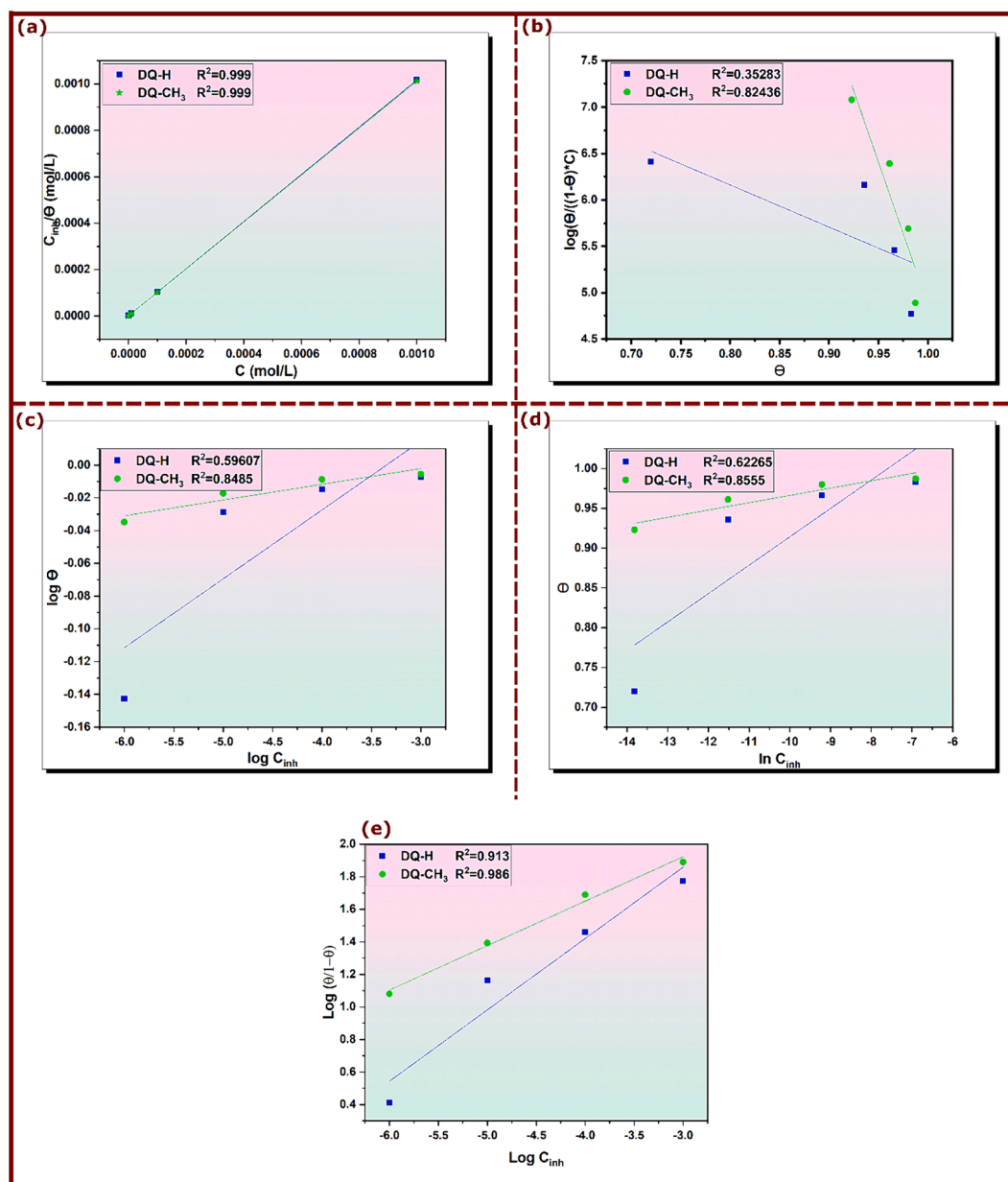


Fig. 7. Langmuir (a), Frumkin (b), Temkin (c), Freundlich (d) and El-Awady (e) adsorption isotherm models of DQ-H and DQ-CH₃ for copper in 3.5% NaCl.

Table 5

Calculated values of standard adsorption parameters of copper corrosion in inhibited solutions.

Inhibitor	Slope	K_{ads} (L.mol ⁻¹)	ΔG_{ads}^0 (kJ.mol ⁻¹)
DQ-H	1.02	112.55×10^4	-44.47
DQ-CH ₃	1.01	273.71×10^4	-46.67

making decisive conclusions about an inhibitor's adsorption mechanism on metal surfaces (Dutta et al., 2017; W. Guo et al., 2020; Tang et al., 2018; Verma et al., 2018b). However, recent studies indicated that this approach is not always true and should be considered with strict precautions (Kokalj, 2022; Walczak et al., 2019). Therefore, adsorption isotherm data are not reported in the present studies and no decisive conclusions about adsorption mechanisms can be made based on adsorption isotherms.

3.6. Surface morphology characterization

The SEM micrographs shown in Fig. 8 provide visual evidence of the effects of quinazolinones on the surface morphology of copper immersed in 3.5 % chloride medium for 72 h at 298 K. Initially, Fig. 8a shows the abraded copper surface, which exhibits a relatively clear surface with minimal scratches resulting from mechanical polishing. This serves as a reference for comparison. In Fig. 8b, where the copper sample was immersed in the blank chloride solution, a significant amount of thick corrosion products is observed, indicating a pronounced dissolution of copper in the chloride medium, in line with the results reported by Guo et al. (Guo et al., 2021).

This observation underlines the aggressive nature of the chloride environment on the copper surface, leading to corrosion. However, after addition of DQ-H and DQ-CH₃, Fig. 8c&8d show a noticeable alteration in copper surface morphology. Here, copper dissolution is noticeably reduced and the metal surface appears smoother compared to the sample immersed in the blank solution. The observed decrease in copper

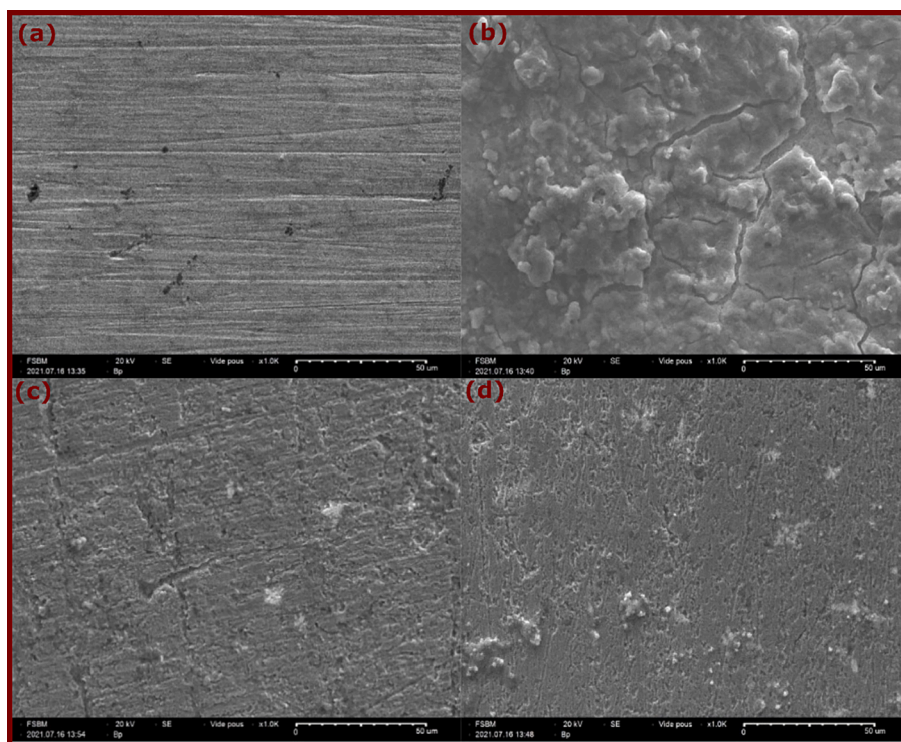


Fig. 8. SEM images of copper (a) polished, (b) after 3 days of immersion in 3.5 % NaCl, (c) and (d) after immersion in 3.5 % NaCl with 10^{-3} mol/L of DQ-H and DQ-CH₃, respectively.

dissolution and smoother surface can be attributed to the formation of a layer of adsorbed inhibitor molecules on the copper surface. This layer acts as a barrier, preventing interaction between the copper surface and the aggressive chloride ions present in the medium (H. Li et al., 2021). Consequently, the inhibitory action of DQ-H and DQ-CH₃ molecules attenuates the corrosion process, preserving the integrity of the copper surface to some extent. While SEM analysis provides visual information on surface morphology and the effects of inhibitors on copper corrosion, complementary spectroscopic techniques such as UV-vis and FT-IR allow further characterization of molecular interactions between inhibitors and the metal surface.

3.7. UV-visible spectroscopy

Complementing the SEM observations, UV-vis spectroscopy provides additional insights into copper-inhibitor interactions in solution. Solutions containing 10^{-3} mol/L of DQ-H and DQ-CH₃ are analyzed

before and after immersion of copper for three days, and results are shown in Fig. 9. Before immersion of the metallic sample, the UV-vis spectra of DQ-H and DQ-CH₃ solutions show absorption peaks at 266 nm and 278 nm for DQ-H and DQ-CH₃, respectively. These absorption bands characterize π - π^* transitions in aromatic rings that are present in the molecular structure of the inhibitors (Singh et al., 2011). However, a displacement in the absorption bands was observed after immersion of copper samples in solutions containing inhibitors, leading to a shift from 266 nm to 279.34 nm for DQ-H and from 278 nm to 284 nm for DQ-CH₃. Furthermore, a decrease in the intensity of the absorption bands accompanies this shift, suggesting the formation of an inhibitor film on the copper surface (H. Li et al., 2021). In other words, the shift in spectral wavelength position (λ) in solutions of these compounds is often interpreted as an indication of the formation of Cu-inhibitor complexes (Yadav and Quraishi, 2012).

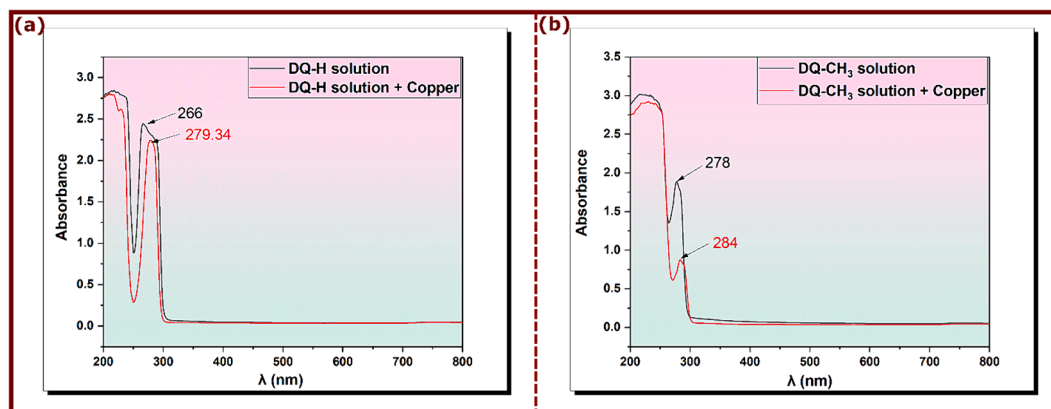


Fig. 9. UV-Vis spectra of 3.5 % NaCl solution with 10^{-3} mol/L of (a) DQ-H and (b) DQ-CH₃ before and after immersion of copper sample for 72 h at 298 K.

3.8. FT-IR spectroscopic measurements

FT-IR spectroscopic assessments have been carried out to ensure the existence of inhibitor film on the copper surface. Fig. 10 represents FT-IR results of pure DQ-H and DQ-CH₃ which have likely the same plots with a slight difference in some band's positions. O-H stretching vibration appears at 3420 cm⁻¹ and 3438 cm⁻¹ for DQ-H and DQ-CH₃, respectively. The adsorption bands at 2985–2937 and 2833 cm⁻¹ are assigned to C-H stretching vibration for DQ-CH₃, while the same bands appear at 2929 cm⁻¹ and 2854 cm⁻¹ for DQ-H. The broad bands 1679 cm⁻¹ and 1685 cm⁻¹ are attributed to C = O. The peaks at 1371 cm⁻¹ and 1380 cm⁻¹ are ascribed to the bending vibration of C-H (Hrimla et al., 2021). A comparison of the FTIR spectra of pure products with those of the scraped material obtained from the copper surface after being submerged in 3.5 % NaCl in the presence of DQ-H and DQ-CH₃ shows that the absorption bands of hydroxyl are shifted from 3420 to 3434 cm⁻¹ and from 3438 to 3463 cm⁻¹ for DQ-H and DQ-CH₃, respectively. Also, the frequency for C = O is moved from 1679 cm⁻¹ to 1675 cm⁻¹ and from 1685 cm⁻¹ to 1632 cm⁻¹, respectively, for DQ-H and DQ-CH₃. Thus, FTIR spectra of pure DQ-H and DQ-CH₃ and their scratches from the copper surface have the same groups and differ only in wavenumbers indicating that the π^* electrons of these groups are involved in the inhibitor adsorption process (Kathiravan et al., 2021). These results reinforce what has been obtained by the above techniques about the existence of a chemical interaction between copper and the molecules of the inhibitor (Zhang et al., 2018c).

3.9. Quantum chemical calculations

Quantum chemical (QC) calculations have been changing the traditional research in corrosion inhibition studies in recent decades (Obot et al., 2015). QC calculations can effectively predict the electronic features and reactivity of compounds, which can clarify the mechanism underlying their interactions with other chemical species. In this regard, global reactivity descriptors such as HOMO, LUMO, and energy gap have been extensively used to predict the adsorption strength of corrosion inhibitors (Lgaz et al., 2021). Although these parameters have limited prediction accuracy because it provides information about the reactivity of individual molecules, they still can be of benefit in terms of predicting adsorption sites and electronic behavior of compounds, particularly when complemented with advanced simulation models such as first-principles DFT calculations. From experimental tests, it has been demonstrated that investigated compounds exhibit similar corrosion inhibition behavior when added to 3.5 wt% NaCl, maintaining higher protection of copper. Numerically, both compounds showed almost equal inhibition efficiency values from weight loss and electrochemical measurements. Therefore, we suppose that the additional methyl group in DQ-CH₃ has no significant effect on the adsorption

abilities of tested compounds. In this section, it would be interesting to investigate the effect of this small structural difference on the electronic and charge distributions of DQ-H and DQ-CH₃ compounds. Fig. 11 represents the optimized molecular structure of DQ-H and DQ-CH₃ and iso-surfaces of HOMO and LUMO densities. It can be observed from optimized molecular structures that both molecules have almost the same geometry and no serious structural changes are noticed. Moving to HOMO and LUMO densities, it can be said that the quinoxalino core is the main part where electron-donating and electron-accepting power of molecules exist. It is well-known that HOMO density is related to the electron-donating ability of molecules while the LUMO density is associated with electron-accepting tendency (Ebenso et al., 2021). Quinoxalino moiety with its heteroatoms and π -systems of aromatic rings can effectively participate in interactions with accepting chemical species such as vacant *d*-orbitals of copper, which if happened, would play a crucial role in the stabilization of molecules-copper interactions. Numerical values of HOMO and LUMO energies and other related quantum chemical parameters are listed in Table 6. Unsurprisingly, numerical values are in line with conclusions made from graphical representation. That is the reactivity descriptors of DQ-H and DQ-CH₃ show almost identical values with no significant differences. It highlights the excellent corrosion inhibition effect of both compounds on the copper corrosion in 3.5 wt% NaCl that is attributed to their electron-rich molecular structures.

To get more insights into the reactivity and the most reactive sites of investigated molecules, Fukui functions are computed and visualized by iso-surfaces in Fig. 12. Fukui functions (FFs) are one of the most useful DFT-derived reactivity indices (Thanikaivelan et al., 2002). FFs have been successfully used to characterize the capacity of molecules, and particularly atoms of molecules to accept or donate electrons; in other words, the tendency of an atom to have a nucleophilic or electrophilic character (De Proft, 2022; Gannouni et al., 2023). The site where the f_k^+ is maximum indicates a high electrophilic property (susceptible to nucleophilic attacks) while the highest f_k^- means that the atomic site has a high nucleophilic character (susceptible to electrophilic attacks) (Saha et al., 2016). From the graphical representation of FFs in Fig. 12, it can be observed that nucleophilic and electrophilic sites are distributed on the entire molecular structure of DQ-H and DQ-CH₃ compounds. However, an inspection of data in Table S1 (supplementary material) reveals that C(16), C(21), O(23) in DQ-CH₃ and N(13), C(20), and C(22) in DQ-H exhibit the highest electrophilic Fukui index f_k^+ , thus acting as preferred atomic sites to accept electrons during a nucleophilic attack (Pareek et al., 2019).

Besides, the electrostatic potential plotted on the optimized molecular structure of molecules is shown in Fig. 12c. It is obvious from the electrostatic potential map that carbonyl and hydroxyl groups represent the more electron-rich regions compared to other parts of the molecules,

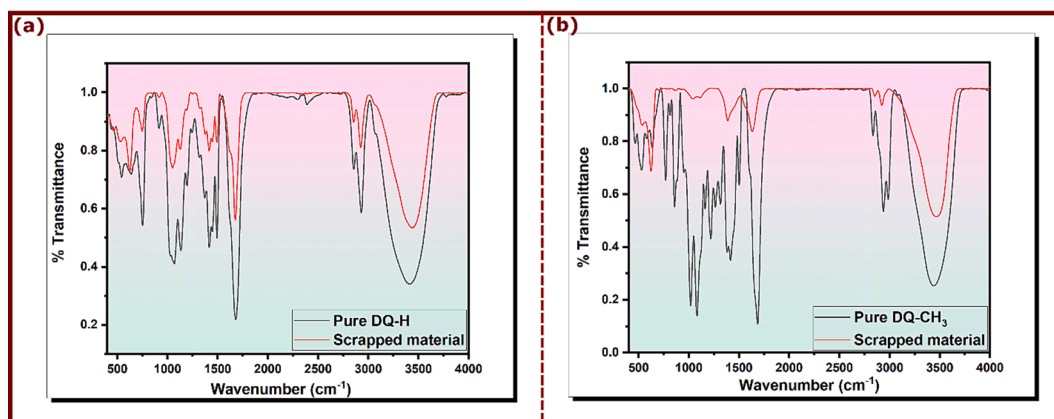


Fig. 10. FT-IR spectra of pure (a) DQ-H and (b) DQ-CH₃ and their scratches from the copper surface in 3.5% NaCl.

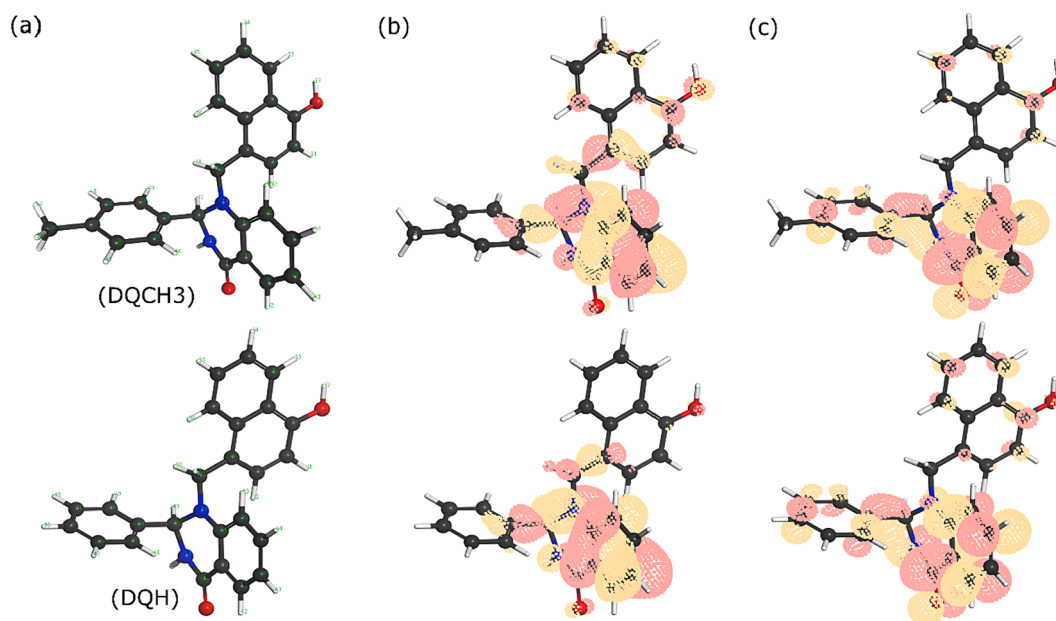


Fig. 11. (a) optimized molecular structures, (b) HOMO, and (c) LUMO iso-surfaces of investigated compounds obtained by DFT/GGA method.

Table 6

Quantum chemical parameters of neutral and protonated pyridine oximes calculated using DFT/GGA method.

Molecule	E_{HOMO}	E_{LUMO}	ΔE	η	ω	σ	ΔN	ϵ
DQ-CH ₃	-5.013	-2.24	2.773	1.386	4.742	0.721	0.430	0.210
DQ-CH	-5.115	-2.243	2.872	1.436	4.712	0.696	0.397	0.212

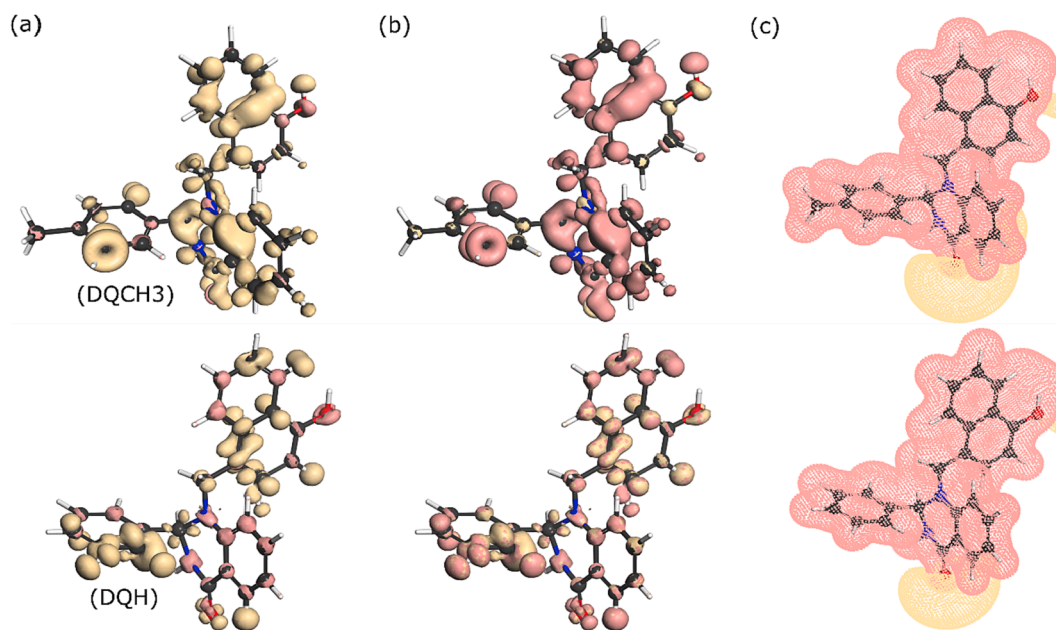


Fig. 12. Iso-surfaces of Fukui functions plotted on molecular structures of DQ-H and DQ-CH₃ (a) f^+ , (b) f^- and (c) molecular electrostatic potential maps.

which indicates that they can be highly reactive adsorption sites when interacting with copper atoms.

3.10. First-principles DFT simulation

3.10.1. Geometries and interaction energies

First-principles calculations are increasingly taking place in different

research fields thanks to the significant development of computer power. An unprecedented level of accuracy can now be achieved for complex simulation systems (Li et al., 2021). In corrosion inhibition research, first-principles DFT calculations are one of the most accurate tools to investigate the adsorption characteristics of molecule-metal systems (Kokalj, 2022).

Herein, first-principles DFT calculations are carried out to assess the

adsorption geometries and electronic properties of DQ-H-Cu(111) and DQ-CH₃-Cu(111) adsorption systems. It is well-documented that large-size corrosion inhibitors mostly adopt a parallel adsorption configuration on metal surfaces. In the case of hydroquinazolinones, it would be difficult to guess the most stable adsorption geometries given the presence of three cyclic systems in each molecule: two with two rings and one with phenyl (DQ-H) and methylphenyl (DQ-CH₃). In this situation, three different initial configurations were optimized to get an overall view of the most probable stable adsorption geometries. Fig. 13&14 represent the DFT optimized adsorption geometries of DQ-CH₃ and DQ-

H on Cu(111) surface, respectively. Considering DQ-CH₃-Cu(111) adsorption geometries, it can be observed that in the three configurations, DQ-CH₃ molecule forms bonds with Cu atoms through its carbon and oxygen atoms. Fig. 13a (DQ-CH₃-I) shows an adsorption configuration where the DQ-CH₃ molecule lies parallel to the Cu(111) surface via its methylphenyl and 4-hydroxynaphthalene parts. Carbon atoms of these two moieties form three bonds with Cu atoms with bond distances between 2.285 and 2.327 Å. The adsorption configuration shown in Fig. 13b (DQ-CH₃-II) indicates that only one bond is formed between the oxygen atom of the carbonyl group and Cu atom, with a bond distance of

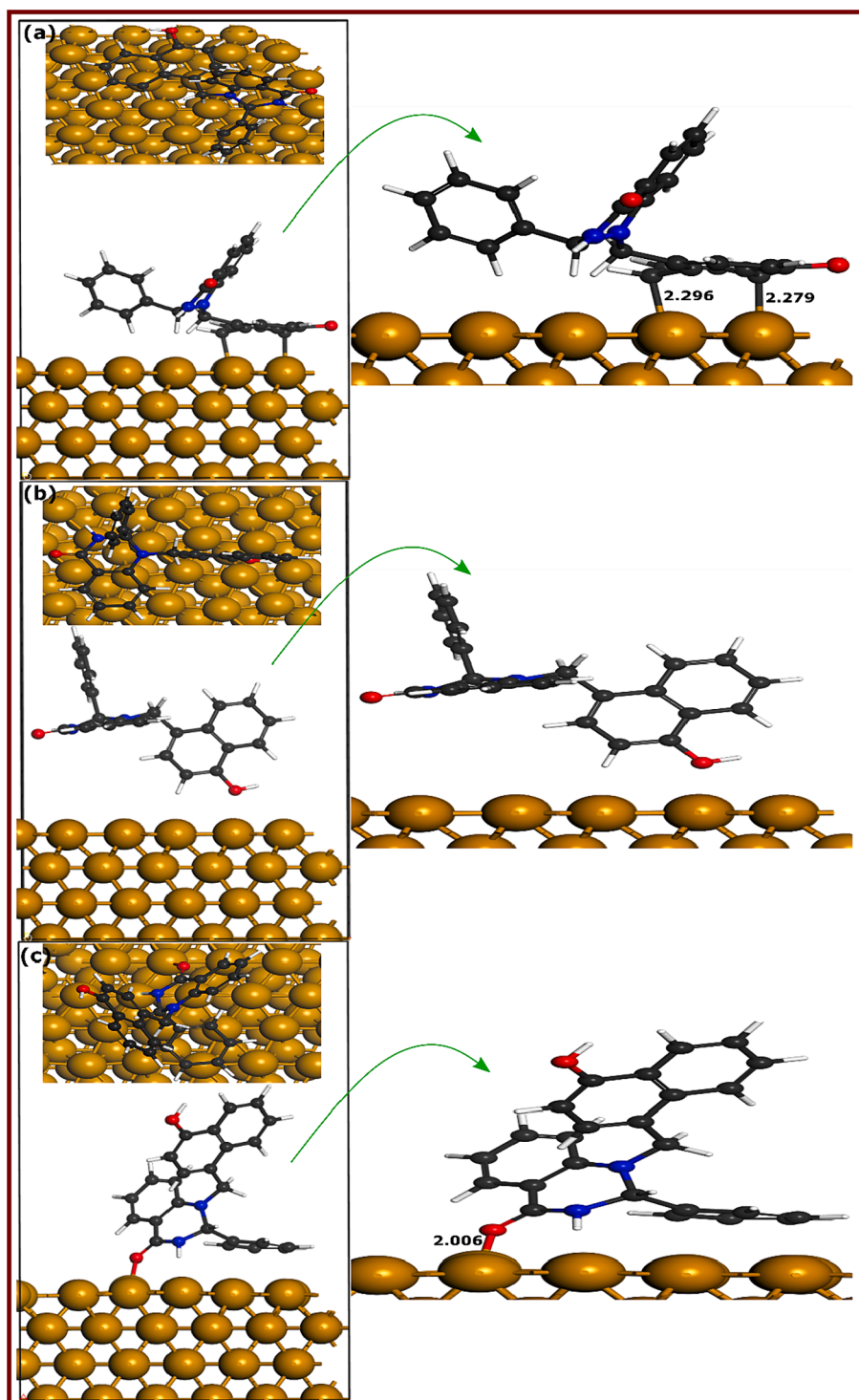


Fig. 13. DFTB-optimized adsorption geometries of DQ-CH₃ at different configurations; (a) Conf.1, (b) Conf. 2, and (c) Conf. 3.

2.024 Å whereas two bonds involving the oxygen atom of the carbonyl group ($O-Cu = 1.974$ Å) and one carbon atom of the methylphenyl moiety ($C-Cu = 2.297$ Å) are observed in adsorption configuration shown in Fig. 13c (DQ-CH₃-III). Moving to DQ-H-Cu(111) adsorption configurations, it can be noticed that opposite to DQ-CH₃-Cu(111) configuration, only 4-hydroxynaphthalene moiety is involved in bonding with Cu atoms as shown in Fig. 14a (DQ-H-I). Two carbons of 4-hydroxynaphthalene moiety are involved in interactions with copper

atoms with bond distances of 2.279 and 2.296 Å. Opposite to DQ-CH₃, the second optimized adsorption geometry of DQ-H-Cu(111) represented in Fig. 14b (DQ-H-II) shows no bonding with copper atoms, while the third adsorption configuration in Fig. 14c (DQ-H-III) reveals the formation of one bond between the oxygen atom of the carbonyl group and copper atoms, having a distance of 2.006 Å. It has been reported that the sum of the covalent radii values for Fe-C ($r_C + r_{Fe}$) and Fe-O ($r_O + r_{Fe}$) are 2.08 and 1.98 Å, respectively (Cordero et al., 2008).

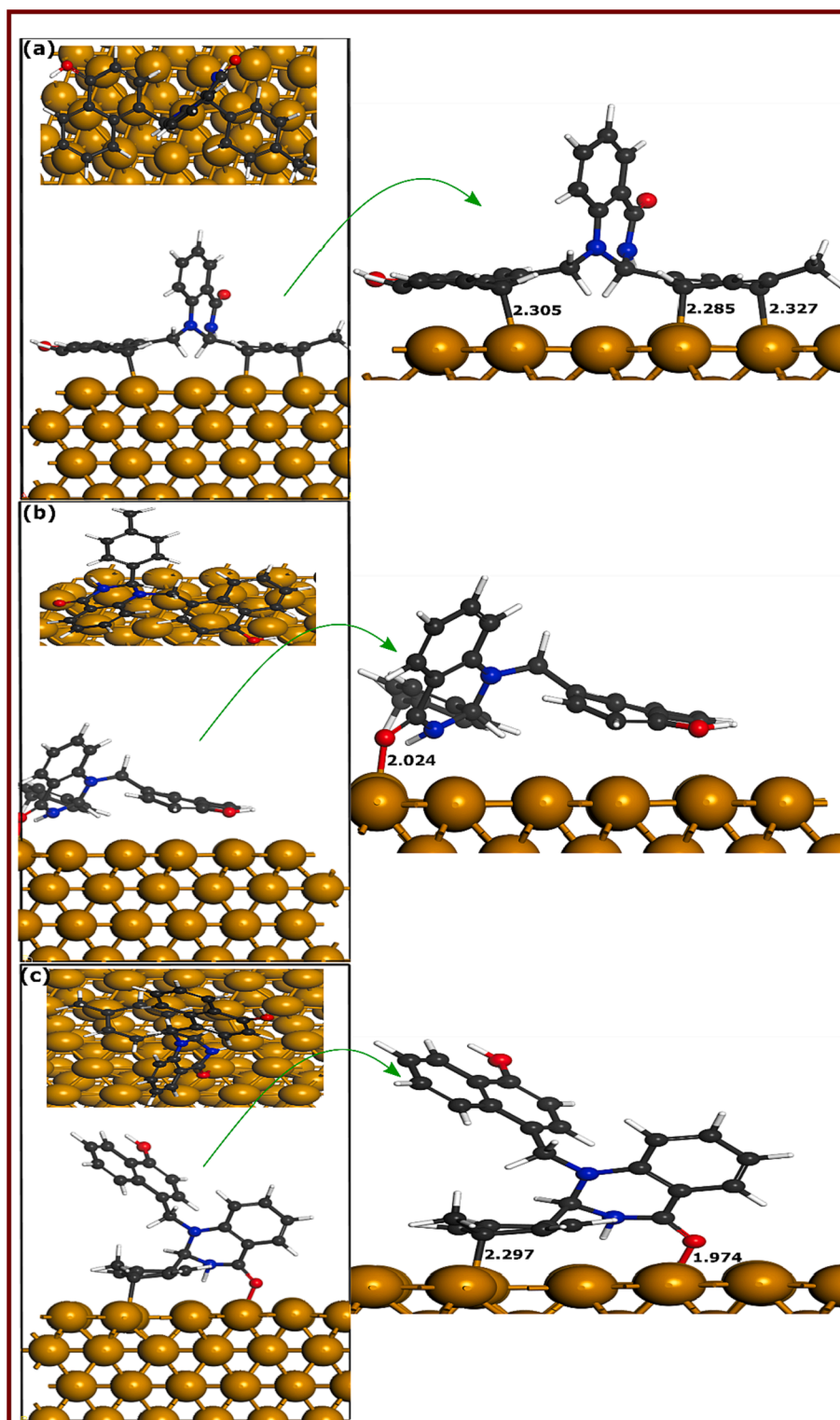


Fig. 14. DFTB-optimized adsorption geometries of DQ-H at different configurations; (a) Conf.1, (b) Conf. 2, and (c) Conf. 3.

It suggests that bonds formed between hydroquinazolinones and Cu (111) surface are covalent.

Despite the fact that experimental evaluations showed similar corrosion inhibition performance, first-principles DFT simulations reveal that the small structural changes resulting from the addition of methyl group have a remarkable effect on the interaction strength with the copper surface. Energetically speaking, analysis of adsorption geometries indicates that DQ-CH₃ configurations have interaction energies of -2.54 , -1.06 , and -2.24 eV for DQ-CH₃-I, DQ-CH₃-II, and DQ-CH₃-III, respectively. Considering DQ-H-Cu(111) adsorption geometries, DQ-H-I, DQ-H-II, and DQ-H-III have interaction energies of -2.07 , -0.033 , and -1.64 eV, respectively. These results further confirm conclusions from optimized adsorption geometries, highlighting the significant effect of the additional methyl group on the adsorption behavior of investigated compounds.

3.10.2. Projected density of states

Deeper insights into the stability of inhibitors' adsorption geometries on Cu(111) can be obtained by electronic structure analysis of inhibitor-Cu(111) in terms of the projected density of states. Projected density of states analysis is a useful tool to get information on the changes in the electronic structure and dominating interactions upon adsorption of DQ-H and DQ-CH₃ on Cu(111) surface (Benbella et al., 2023; Matanou et al., 2023). Figs. 15 & 16 show the projected density of states on *d*-orbitals of Cu atoms and *s*,*p*-orbitals of DQ-CH₃ and DQ-H adsorbed molecules on Cu(111) surface. By comparison with PDOSs of isolated molecules shown in Figs. 15a and 16a, a slight distortion of states is observed for the three adsorption configurations of DQ-CH₃ represented in Figs. 15b-d and 16b-d. After the adsorption of DQ-CH₃ molecules, states are shifted slightly to negative energies, which indicates a strong hybridization of the Cu *d*-states with adsorbate *s*,*p*-states of DQ-H molecules (Benbella et al., 2023). Concerning adsorption configurations of DQ-H-Cu(111), the same conclusions can be made for DQ-H-I and DQ-H-III adsorption configurations, where the energy shift and distortion of states are noticeable. However, a close inspection of PDOS plots of DQ-

H-II reveals no hybridization of states (Benbella et al., 2023). These results strengthen the conclusions made from DFT-optimized adsorption geometries and confirm the chemical action between inhibitors' orbitals and vacant *d*-orbitals of copper as a main mechanism of the corrosion inhibition effect.

4. Conclusions

In the present study, a comprehensive experimental and theoretical characterization of the corrosion inhibition performance and adsorption characteristics of two novel hydroquinazolinones derivatives for copper in 3.5 wt% NaCl. On the basis of the experimental and theoretical results, it could be concluded that:

- (1) Gravimetric analysis, potentiodynamic polarization curves (PPC) and electrochemical impedance spectroscopy (EIS) collectively confirm the robust inhibition capabilities of the quinazolinones studied, as evidenced by inhibition efficiency values exceeding 90 % at a concentration of 10^{-3} mol/L according to all techniques.
- (2) Electrochemical evaluation of corrosion inhibition abilities of DQ-CH₃ and DQ-H compounds revealed an outstanding anti-corrosion effect with inhibition efficiencies reaching 92 % and 94 % for DQ-H and DQ-CH₃, respectively.
- (3) The increase in polarization resistance (R_p) from 3590 to 9403 Ω cm² for DQ-H and from 3811 to 12861 Ω cm² for DQ-CH₃, as the concentration increased from 10^{-6} to 10^{-3} mol/L in the EIS, along with the decrease in corrosion current density (i_{corr}) from 36.8 to 2.17 μ A cm⁻² for DQ-H and from 10.1 to 1.67 μ A cm⁻² for DQ-CH₃ in the PPC, illustrate the preventive properties of DQ-H and DQ-CH₃ against copper corrosion.
- (4) The influence of temperature was further examined by PPC test, and a slight decrease in inhibition efficiency and an increase in corrosion rate were observed with increasing temperature.

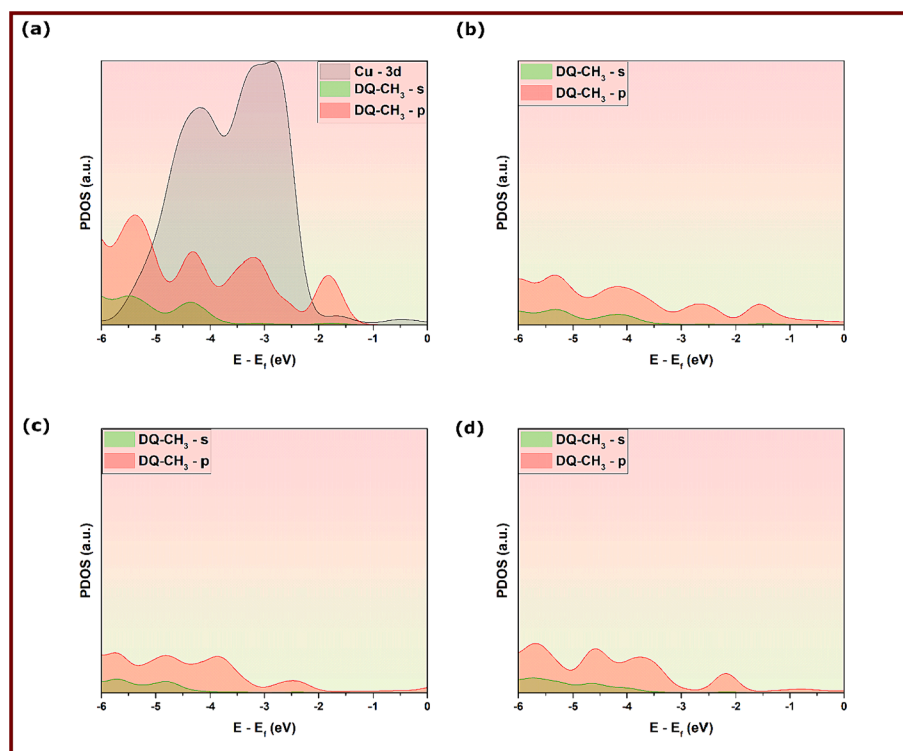


Fig. 15. PDOS analysis of DFTB-optimized adsorption geometries of DQ-CH₃ at different configurations; (a) Before adsorption, (b) Conf. 1, (c) Conf. 2 and (d) Conf. 3.

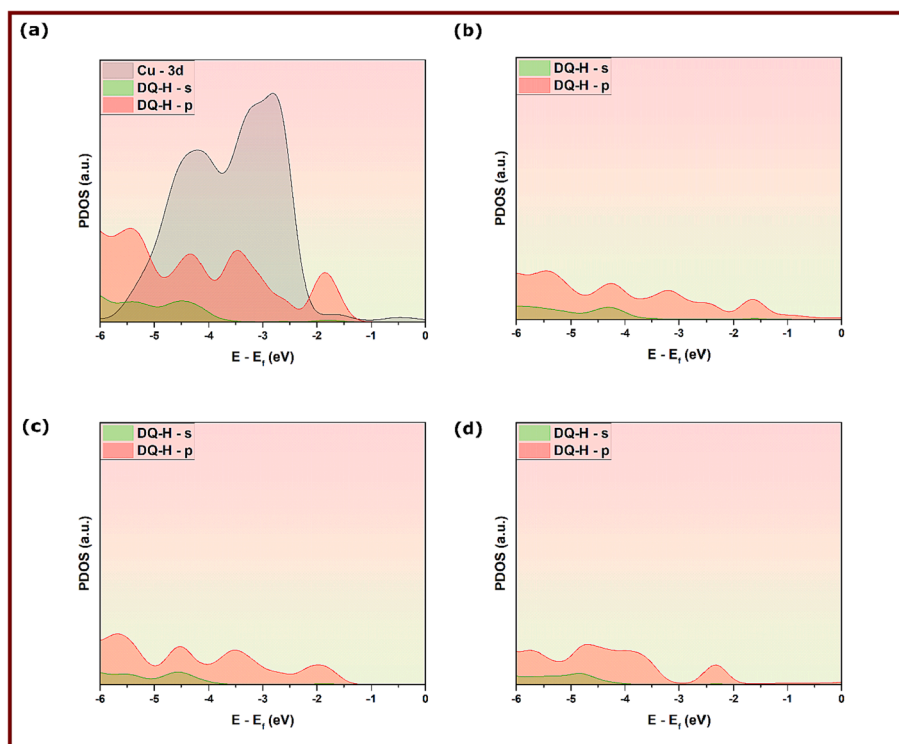


Fig. 16. PDOS analysis of DFTB-optimized adsorption geometries of DQ-H at different configurations; (a) Before adsorption, (b) Conf. 1, (b) Conf. 2 and (c) Conf. 3.

- (5) Despite the incorporation of an additional methyl group in the DQ-CH₃ compound, there was no remarkable effect on the corrosion inhibition performance, and both compounds showed a strong inhibition effect on copper corrosion in 3.5 wt% NaCl.
- (6) SEM analysis revealed a significant improvement in copper surface morphology after the addition of DQ-CH₃ and DQ-H compounds to 3.5 wt% NaCl solutions.
- (7) Conclusions made from FTIR analysis suggested that inhibitor molecules strongly adsorbed on the copper surface, which was further confirmed by UV–vis spectroscopy measurements.
- (8) The DFT optimization of adsorption geometries was carried out for three different configurations of each molecule. It revealed the formation of several covalent bonds between the DQ-CH₃ molecule and copper surface whereas DQ-H showed the formation of covalent bonds only for two adsorption configurations.
- (9) The electronic structure analysis of inhibitor-Cu(1 1 1) adsorption systems affirmed the existence of strong hybridization of the Cu *d*-states with adsorbate *s*,*p*-states of DQ-H and DQ-CH₃ molecules.

Outcomes from the present study provided deeper insights into the corrosion inhibition mechanisms of hydroquinazolinones for copper in 3.5 wt% NaCl, which is believed to fill a gap in the literature on the application of hydroquinazolinones.

CRediT authorship contribution statement

Mohammed Oubahou: Conceptualization, Methodology, Formal analysis, Investigation, Data curation, Writing – original draft. **Mohamed Rbaa:** Conceptualization, Methodology, Formal analysis, Investigation, Data curation, Writing – original draft. **Hassane Lgaz:** Conceptualization, Methodology, Formal analysis, Investigation, Data curation, Writing – original draft. **Driss Takky:** Investigation, Supervision, Visualization, Writing – review & editing. **Youssef Naimi:** Investigation, Supervision, Visualization, Writing – review & editing. **Awad A. Alrashdi:** Project administration, Funding acquisition, Supervision, Writing – review & editing. **Han-seung Lee:** Project administration,

Funding acquisition, Supervision, Writing – review & editing.

Declaration of competing interest

The authors declare that they have no known competing financial interests or personal relationships that could have appeared to influence the work reported in this paper.

Acknowledgment

“This work was supported by the National Research Foundation of Korea (NRF) grant funded by the Korea government (MSIT) (No. NRF-2018R1A5A1025137).”

Appendix A. Supplementary data

Supplementary data to this article can be found online at <https://doi.org/10.1016/j.arabjc.2024.105716>.

References

- A. Aabid, A. A. Jafar, S. Obaid Ahmed, M., & Humadi, J. I. (2021). Inhibitory effect of ceftriaxone sodium on corrosion of copper in 1M nitric acid. *Mater. Today: Proc.*, xxx. Doi: 10.1016/j.matpr.2021.05.345.
- Abbasov, V.M., Abd El-Lateef, H.M., Aliyeva, L.L., Qasimov, E.E., Ismayilov, I.T., Khalaf, M.M., 2013. A study of the corrosion inhibition of mild steel C1018 in CO₂-saturated brine using some novel surfactants based on corn oil. *Egypt. J. Pet.* 22 (4), 451–470. <https://doi.org/10.1016/j.ejpe.2013.11.002>.
- Abd El-Lateef, H.M., Shalabi, K., Tantawy, A.H., 2020. Corrosion inhibition of carbon steel in hydrochloric acid solution using newly synthesized urea-based cationic fluorosurfactants: experimental and computational investigations. *New J. Chem.* 44 (41), 17791–17814. <https://doi.org/10.1039/D0NJ04004E>.
- Abd El-Lateef, H.M., El-Beltagi, H.S., Mohamed Mohamed, M.E., Kandeel, M., Bakir, E., Toghian, A., Shalabi, K., Tantawy, A.H., Khalaf, M.M., 2022. Novel natural surfactant-based fatty acids and their corrosion-inhibitive characteristics for carbon steel-induced sweet corrosion: detailed practical and computational explorations. *Front. Mater.* 9 (February), 1–18. <https://doi.org/10.3389/fmats.2022.843438>.
- Abdelsattar, M., Badawi, A.E.F.M., Ibrahim, S., Wasfy, A.F., Tantawy, A.H., Dardir, M.M., 2020. Corrosion control of carbon steel in water-based mud by nanosized meallo-cationic surfactant complexes during drilling operations. *ACS Omega* 5 (48), 30881–30897. <https://doi.org/10.1021/acsomega.0c03653>.

- Ahmad, Z., 2006. CHAPTER 1 - introduction to corrosion. In: Ahmad, Z. (Ed.), Principles of Corrosion Engineering and Corrosion Control. Butterworth-Heinemann, pp. 1–8. <https://doi.org/10.1016/B978-075065924-6/50002-7>.
- Akinbulumo, O. A., Odejobi, O. J., & Odekanle, E. L. (2020). Thermodynamics and adsorption study of the corrosion inhibition of mild steel by Euphorbia heterophylla L. extract in 1.5 M HCl. Results in Materials, 5(October 2019), 100074. Doi: 10.1016/j.rinma.2020.100074.
- Al Jahdaly, B.A., Maghraby, Y.R., Ibrahim, A.H., Shouier, K.R., Alturki, A.M., El-Shabasy, R.M., 2022. Role of green chemistry in sustainable corrosion inhibition: a review on recent developments. Mater. Today Sustain. 20, 100242 <https://doi.org/10.1016/j.mtsust.2022.100242>.
- Alaoui, K., Ouakki, M., Abousalem, A.S., Serrar, H., Galai, M., Derbali, S., Nouneh, K., Boukhris, S., Touhami, M.E., El Kacimi, Y., 2019. Molecular dynamics, Monte-Carlo simulations and atomic force microscopy to study the interfacial adsorption behaviour of some triazepine carboxylate compounds as corrosion inhibitors in acid medium. J. Bio- and Tribo-Corrosion 5 (1). <https://doi.org/10.1007/s40735-018-0196-2>.
- Al-Azawi, K.F., Mohammed, I.M., Al-Baghdadi, S.B., Salman, T.A., Issa, H.A., Al-Amriy, A.A., Gaaz, T.S., Kadhum, A.A.H., 2018. Experimental and quantum chemical simulations on the corrosion inhibition of mild steel by 3-(5-(3,5-dinitrophenyl)-1,3,4-thiadiazol-2-yl)imino)indolin-2-one. Results Phys. 9, 278–283. <https://doi.org/10.1016/j.rinp.2018.02.055>.
- Aldana-gonzález, J., Cervantes-cuevas, H., Alfaro-romo, C., Rodríguez-clemente, E., Uruchurtu-chavarín, J., 2020. Experimental and theoretical study on the corrosion inhibition of API 5L X52 steel in acid media by a new quinazolinone derivative. J. Mol. Liq. 320, 114449 <https://doi.org/10.1016/j.molliq.2020.114449>.
- Alsibaee, A.M., Al-Yousef, H.M., Al-Salem, H.S., 2023. Quinazolinones, the winning horse in drug discovery. Molecules 28 (3). <https://doi.org/10.3390/molecules28030978>.
- Ansari, A., Ou-Ani, O., Oucheikh, L., Youssefi, Y., Chebabe, D., Oubair, A., Znini, M., 2022. Experimental, theoretical modeling and optimization of inhibitive action of Ocimum basilicum essential oil as green corrosion inhibitor for C38 steel in 0.5 M H2SO4 medium. chemistry. Africa 5 (1), 37–55. <https://doi.org/10.1007/s42250-021-00289-x>.
- Arrousse, N., Salim, R., Bousraf, F.Z., Ech-chihbi, E., Hammouti, B., Abdellaoui, A., El Hajjaji, F., Taleb, M., 2022. Experimental and theoretical study of xanthene derivatives as corrosion inhibitor for mild steel in hydrochloric acid solution. J. Appl. Electrochem. 52 (8), 1275–1294. <https://doi.org/10.1007/s10800-022-01705-x>.
- Ashassi-Sorkhabi, H., Shaabani, B., Seifzadeh, D., 2005. Corrosion inhibition of mild steel by some Schiff base compounds in hydrochloric acid. Appl. Surf. Sci. 239 (2), 154–164. <https://doi.org/10.1016/j.apsusc.2004.05.143>.
- Ayati, N.S., Khandandel, S., Momeni, M., Moayed, M.H., Davoodi, A., Rahimizadeh, M., 2011. Inhibitive effect of synthesized 2-(3-pyridyl)-3,4-dihydro-4-quinazolinone as a corrosion inhibitor for mild steel in hydrochloric acid. Mater. Chem. Phys. 126 (3), 873–879. <https://doi.org/10.1016/j.matchemphys.2010.12.023>.
- Belghiti, M., Benhiba, F., Benzbiria, N., Lai, C.-H., Echihi, S., Salah, M., Zeroual, A., Karzazi, Y., Tounsi, A., Abbiche, K., Belaouad, S., Elaloui-Elabdallaoui, H., Naimi, Y., 2022. Performance of triazole derivatives as potential corrosion inhibitors for mild steel in a strong phosphoric acid medium: combining experimental and computational (DFT, MDs & QSAR) approaches. J. Mol. Struct. 1256, 132515 <https://doi.org/10.1016/j.molstruc.2022.132515>.
- Belghiti, M.E., Karzazi, Y., Dafali, A., Obot, I.B., Ebenso, E.E., Emran, K.M., Bahadur, I., Hammouti, B., Bentiss, F., 2016. Anti-corrosive properties of 4-amino-3,5-bis (disubstituted)-1,2,4-triazole derivatives on mild steel corrosion in 2 M H3PO4 solution: experimental and theoretical studies. J. Mol. Liq. 216, 874–886. <https://doi.org/10.1016/j.molliq.2015.12.093>.
- Belhadi, M., Oubahou, M., Hammoudan, I., Chakra, A., Chafi, M., Tighadouini, S., 2023. A comprehensive assessment of carbon steel corrosion inhibition by 1,10-phenanthroline in the acidic environment: insights from experimental and computational studies. Environ. Sci. Pollut. Res. <https://doi.org/10.1007/s11356-023-27582-1>.
- Benbouguerra, K., Chafaa, S., Chafai, N., Mehri, M., Moumeni, O., Hellal, A., 2018. Synthesis, spectroscopic characterization and a comparative study of the corrosion inhibitive efficiency of an α -aminophosphonate and Schiff base derivatives: experimental and theoretical investigations. J. Mol. Struct. 1157, 165–176. <https://doi.org/10.1016/j.molstruc.2017.12.049>.
- Bentiss, F., Lebrini, M., Lagrenée, M., Traisnel, M., Elfarouk, A., Vezin, H., 2007. The influence of some new 2,5-disubstituted 1,3,4-thiadiazoles on the corrosion behaviour of mild steel in 1 M HCl solution: AC impedance study and theoretical approach. Electrochim. Acta 52 (24), 6865–6872. <https://doi.org/10.1016/j.electacta.2007.04.111>.
- Boudjellal, F., Ouici, H.B., Guendouzi, A., Benali, O., Sehmi, A., 2020. Experimental and theoretical approach to the corrosion inhibition of mild steel in acid medium by a newly synthesized pyrazole carbothioamide heterocycle. J. Mol. Struct. 1199, 127051 <https://doi.org/10.1016/j.molstruc.2019.127051>.
- Bourzami, R., Ouksel, L., Chafai, N., 2019. Synthesis, spectral analysis, theoretical studies, molecular dynamic simulation and comparison of anticorrosive activity of an ester and an acid α -hydroxyphosphonates. J. Mol. Struct. 1195, 839–849. <https://doi.org/10.1016/j.molstruc.2019.06.012>.
- Chafai, N., Chafaa, S., Benbouguerra, K., Daoud, D., Hellal, A., Mehri, M., 2017. Synthesis, characterization and the inhibition activity of a new α -aminophosphonic derivative on the corrosion of XC48 carbon steel in 0.5 M H2SO4: experimental and theoretical studies. J. Taiwan Inst. Chem. Eng. 70, 331–344. <https://doi.org/10.1016/j.tice.2016.10.026>.
- Chafai, N., Chafaa, S., Benbouguerra, K., Hellal, A., Mehri, M., 2019. Synthesis, spectral analysis, anti-corrosive activity and theoretical study of an aromatic hydrazone derivative. J. Mol. Struct. 1181, 83–92. <https://doi.org/10.1016/j.molstruc.2018.12.073>.
- Chauki, A., Chafiq, M., Rbaa, M., Lgaz, H., Salghi, R., Lakhrissi, B., Ali, I.H., Masroor, S., Cho, Y., 2020a. New 8-hydroxyquinoline-bearing quinoxaline derivatives as effective corrosion inhibitors for mild steel in HCl: electrochemical and computational investigations. Coatings 10 (9). <https://doi.org/10.3390/coatings10090811>.
- Chauki, A., Chafiq, M., Rbaa, M., Salghi, R., Lakhrissi, B., Ali, I.H., Bashir, S., Chung, I. M., 2020b. Comprehensive assessment of corrosion inhibition mechanisms of novel benzimidazole compounds for mild steel in HCl: an experimental and theoretical investigation. J. Mol. Liq. 320 <https://doi.org/10.1016/j.molliq.2020.114383>.
- Chauhan, D.S., Quraishi, M.A., Carrière, C., Seyeux, A., Marcus, P., Singh, A., 2019. Electrochemical, ToF-SIMS and computational studies of 4-amino-5-methyl-4H-1,2,4-triazole-3-thiol as a novel corrosion inhibitor for copper in 3.5% NaCl. J. Mol. Liq. 289 <https://doi.org/10.1016/j.molliq.2019.111113>.
- Chen, W., Nie, B., Liu, M., Li, H.J., Wang, D.Y., Zhang, W., Wu, Y.C., 2021a. Mitigation effect of quinazolin-4(3H)-one derivatives on the corrosion behaviour of mild steel in HCl. Colloids Surf. A Physicochem. Eng. Asp. 627 <https://doi.org/10.1016/j.colsurfa.2021.127188>.
- Chen, S., Xiang, B., Chen, S., Zou, X., Zhou, Y., Hou, J., 2018. Synthesis and surface characterization of self-assembled monolayers of thiazoles incorporating hydrocarbon and fluorocarbon chains on copper substrates. Appl. Surf. Sci. 456 (May), 25–36. <https://doi.org/10.1016/j.apsusc.2018.06.082>.
- Clark, S.J., Segall, M.D., Pickard, C.J., Hasnip, P.J., Probert, M.L.J., Refson, K., Payne, M. C., 2005. First principles methods using CASTEP. Z. Kristallogr. 220 (5–6), 567–570. <https://doi.org/10.1524/zkri.220.5.567.65075>.
- Dafali, A., Hammouti, B., Mokhlisse, R., Kertit, S., 2003. Substituted uracils as corrosion inhibitors for copper in 3% NaCl solution. Corros. Sci. 45 (8), 1619–1630. [https://doi.org/10.1016/S0010-938X\(02\)00255-X](https://doi.org/10.1016/S0010-938X(02)00255-X).
- Damej, M., Kaya, S., EL Ibrahim, B., Lee, H. S., Molhi, A., Serdaroglu, G., Benmessaoud, M., Ali, I. H., EL Hajjaji, S., & Lgaz, H. (2021). The corrosion inhibition and adsorption behavior of mercaptobenzimidazole and bis-mercaptobenzimidazole on carbon steel in 1.0 M HCl: Experimental and computational insights. Surfaces and Interfaces, 24(December 2020). Doi: 10.1016/j.surf.2021.101095.
- De Souza, F.S., Spinelli, A., 2009. Caffeic acid as a green corrosion inhibitor for mild steel. Corros. Sci. 51 (3), 642–649. <https://doi.org/10.1016/j.corsci.2008.12.013>.
- Deslouis, C., Tribollet, B., Mengoli, G., Musiani, M.M., 1988. Electrochemical behaviour of copper in neutral aerated chloride solution. II. impedance investigation. J. Appl. Electrochem. 18 (3), 384–393. <https://doi.org/10.1007/BF01093752>.
- Djenane, M., Chafaa, S., Chafai, N., Kerkour, R., Hellal, A., 2019. Synthesis, spectral properties and corrosion inhibition efficiency of new ethyl hydrogen [(methoxyphenyl) (methylamino) methyl] phosphonate derivatives: experimental and theoretical investigation. J. Mol. Struct. 1175, 398–413. <https://doi.org/10.1016/j.molstruc.2018.07.087>.
- Dutta, A., Saha, S.K., Adhikari, U., Banerjee, P., Sukul, D., 2017. Effect of substitution on corrosion inhibition properties of 2-(substituted phenyl) benzimidazole derivatives on mild steel in 1 M HCl solution: a combined experimental and theoretical approach. Corros. Sci. 123 (April), 256–266. <https://doi.org/10.1016/j.corsci.2017.04.017>.
- Ebenso, E.E., Verma, C., Olasunkanmi, L.O., Akpan, E.D., Verma, D.K., Lgaz, H., Guo, L., Kaya, S., Quraishi, M.A., 2021. Molecular modelling of compounds used for corrosion inhibition studies: a review. Phys. Chem. Chem. Phys. 23 (36), 19987–20027. <https://doi.org/10.1039/D1CP00244A>.
- El, A., Mohammed, A., Abdeslam, O., Bouari, E., Tanane, O., 2023. Expired amoxicillin as an eco - friendly corrosion inhibitor for cast steel in sulfuric acid environment : electrochemical, surface and thermodynamic studies. J. Solid State Electrochem. 0123456789 <https://doi.org/10.1007/s10008-023-05788-0>.
- El-Awady, A.A., Abd-El-Nabey, B.A., Aziz, S.G., Khalifa, M., Al-Ghamedy, H.A., 1990. Kinetics and thermodynamics of the inhibition of the acid corrosion of steel by some macrocyclic ligands. Int. J. Chem 1 (4), 169–179.
- El-Haddad, M.N., Fouda, A.S., 2015. Electroanalytical, quantum and surface characterization studies on imidazole derivatives as corrosion inhibitors for aluminum in acidic media. J. Mol. Liq. 209, 480–486. <https://doi.org/10.1016/j.molliq.2015.06.005>.
- El-Hajjaji, F., Belghiti, M.E., Hammouti, B., Jodeh, S., Hamed, O., Lgaz, H., Salghi, R., 2018. Adsorption and corrosion inhibition effect of 2-mercaptobenzimidazole (surfactant) on a carbon steel surface in an acidic medium: experimental and Monte Carlo simulations. Port. Electrochim. Acta 36 (3), 197–212. <https://doi.org/10.4152/pea.201803197>.
- El-Hajjaji, F., Ech-chihbi, E., Rezki, N., Benhiba, F., Taleb, M., Chauhan, D.S., Quraishi, M.A., 2020. Electrochemical and theoretical insights on the adsorption and corrosion inhibition of novel pyridinium-derived ionic liquids for mild steel in 1 M HCl. J. Mol. Liq. 314, 113737 <https://doi.org/10.1016/j.molliq.2020.113737>.
- Errahmany, N., Rbaa, M., Abousalem, A.S., Tazouti, A., Galai, M., El Kafsaoui, E.H., Touhami, M.E., Lakhrissi, B., Tuir, R., 2020. Experimental, DFT calculations and MC simulations concept of novel quinazolinone derivatives as corrosion inhibitor for mild steel in 1.0 M HCl medium. J. Mol. Liq. 312, 113413 <https://doi.org/10.1016/j.molliq.2020.113413>.
- Faydy, M. El, Rbaa, M., Lakhrissi, L., Lakhrissi, B., Warad, I., Zarrouk, A., & Obot, I. B. (2019). Corrosion protection of carbon steel by two newly synthesized benzimidazole-2-ones substituted 8-hydroxyquinoline derivatives in 1 M HCl: Experimental and theoretical study. Surfaces and Interfaces, 14(October 2018), 222–237. Doi: 10.1016/j.surf.2019.01.005.
- Finsgar, M., Milošev, I., 2010. Inhibition of copper corrosion by 1,2,3-benzotriazole: a review. Corros. Sci. 52 (9), 2737–2749. <https://doi.org/10.1016/j.corsci.2010.05.002>.

- Fouda, A.-E.-A.-S., Abdallah, M., El-Dahab, R.A., 2010. Some quinazoline derivatives as corrosion inhibitors for copper in HNO₃ solution. *Desalin. Water Treat.* 22, 340–348. <https://api.semanticscholar.org/CorpusID:97967196>.
- Fouda, A.S., Hassan, H.M., 2013. Quinazoline derivatives as green corrosion inhibitors for carbon steel in hydrochloric acid solutions. *Int. J. Electrochem. Sci.* 8 (4), 5866–5885. [https://doi.org/10.1016/S1452-3981\(23\)14728-6](https://doi.org/10.1016/S1452-3981(23)14728-6).
- Fukui, K., 1982. The role of frontier orbitals in chemical reactions (nobel lecture). *Angew. Chem. Int. Ed. Eng.* 21 (11), 801–809. <https://doi.org/10.1002/anie.198208013>.
- Gad Allah, A.G., Hefny, M.M., Salih, S.A., El-Basiouny, M.S., 1989. Corrosion inhibition of zinc in HCl solution by several pyrazole derivatives. *Corrosion* 45 (7), 574–578. <https://doi.org/10.5006/1.3577875>.
- Galai, M., Rbaa, M., Ouakki, M., Abousalem, A.S., Ech-chihbi, E., Dahmani, K., Dkhireche, N., Lakhri, B., EbnTouhami, M., 2020. Chemically functionalized of 8-hydroxyquinoline derivatives as efficient corrosion inhibition for steel in 1.0 M HCl solution: experimental and theoretical studies. *Surf. Interfaces* 21 (September), 100695. <https://doi.org/10.1016/j.surfint.2020.100695>.
- Galai, M., Rbaa, M., Ouakki, M., Guo, L., Dahmani, K., Nouneh, K., Briche, S., Lakhri, B., Dkhireche, N., Ebn Touhami, M., 2021. Effect of alkyl group position on adsorption behavior and corrosion inhibition of new naphthol based on 8-hydroxyquinoline: electrochemical, surface, quantum calculations and dynamic simulations. *J. Mol. Liq.* 335, 116552. <https://doi.org/10.1016/j.molliq.2021.116552>.
- Gao, H., Xie, N., Wang, H., Chen, M., Zhang, J., Sun, J., Jin, Z., 2020. Evaluation of corrosion inhibition performance of a novel ionic liquid based on synergism between cation and anion. *New J. Chem.* 44 (19), 7802–7810. <https://doi.org/10.1039/D0NJ00745E>.
- Giri, R.S., Thaker, H.M., Giordano, T., Williams, J., Rogers, D., Sudersanam, V., Vasu, K. K., 2009. Design, synthesis and characterization of novel 2-(2,4-disubstituted-thiazole-5-yl)-3-aryl-3H-quinazolin-4-one derivatives as inhibitors of NF- κ B and AP-1 mediated transcription activation and as potential anti-inflammatory agents. *Eur. J. Med. Chem.* 44 (5), 2184–2189. <https://doi.org/10.1016/j.ejmech.2008.10.031>.
- Guo, X., Huang, H., Liu, D., 2021. The inhibition mechanism and adsorption behavior of three purine derivatives on the corrosion of copper in alkaline artificial seawater: structure and performance. *Colloids Surf. A Physicochem. Eng. Asp.* 622 (February), 126644. <https://doi.org/10.1016/j.colsurfa.2021.126644>.
- Guo, W., Umar, A., Zhao, Q., Alsaiani, M.A., Al-Hadeethi, Y., Wang, L., Pei, M., 2020. Corrosion inhibition of carbon steel by three kinds of expired cephalosporins in 0.1 M H₂SO₄. *J. Mol. Liq.* 320, 114295. <https://doi.org/10.1016/j.molliq.2020.114295>.
- Hamdy, A., El-Gendy, N.S., 2013. Thermodynamic, adsorption and electrochemical studies for corrosion inhibition of carbon steel by henna extract in acid medium. *Egypt. J. Pet.* 22 (1), 17–25. <https://doi.org/10.1016/j.ejpe.2012.06.002>.
- Harvey, T.G., Hardin, S.G., Hughes, A.E., Muster, T.H., White, P.A., Markley, T.A., Corrigan, P.A., Mardel, J., Garcia, S.J., Mol, J.M.C., Glenn, A.M., 2011. The effect of inhibitor structure on the corrosion of AA2024 and AA7075. *Corros. Sci.* 53 (6), 2184–2190. <https://doi.org/10.1016/j.corsci.2011.02.040>.
- He, J., Li, Q., Li, X., An, J., Chen, G., Zhao, L., Li, W., 2020. Insight into the anti-corrosion mechanism of 2-aminobenzenethiol as the inhibitor for copper in acid environment. *J. Mol. Liq.* 320, 114494. <https://doi.org/10.1016/j.molliq.2020.114494>.
- Hong, S., Chen, W., Luo, H.Q., Li, N.B., 2012. Inhibition effect of 4-amino-antipyrine on the corrosion of copper in 3wt% NaCl solution. *Corros. Sci.* 57, 270–278. <https://doi.org/10.1016/j.corsci.2011.12.009>.
- Hrimla, M., Bahsis, L., Boutouil, A., Laamari, M.R., Julve, M., Stiriba, S.E., 2021. Corrosion inhibition performance of a structurally well-defined 1,2,3-triazole derivative on mild steel-hydrochloric acid interface. *J. Mol. Struct.* 1231, 129895. <https://doi.org/10.1016/j.molstruc.2021.129895>.
- Huang, H., Guo, X., 2020. The relationship between the inhibition performances of three benzo derivatives and their structures on the corrosion of copper in 3.5 wt.% NaCl solution. *Colloids Surf. A Physicochem. Eng. Asp.* 598 (January), 124809. <https://doi.org/10.1016/j.colsurfa.2020.124809>.
- Isin, D.O., Karakus, N., 2015. Quantum chemical study on the inhibition efficiencies of some sym-triazines as inhibitors for mild steel in acidic medium. *J. Taiwan Inst. Chem. Eng.* 50, 306–313. <https://doi.org/10.1016/j.jtice.2014.12.035>.
- Jafari, E., Khajouei, M.R., Hassanzadeh, F., Hakimelahi, G.H., Khodarahmi, G.A., 2016. Quinazolinone and quinazoline derivatives: recent structures with potent antimicrobial and cytotoxic activities. *Res. Pharm. Sci.* 11 (1), 1–14.
- Kannan, P., Rao, T.S., Rajendran, N., 2018. Improvement in the corrosion resistance of carbon steel in acidic condition using naphthalen-2-yl-naphthalene-2-carboxamide inhibitor. *J. Colloid Interface Sci.* 512, 618–628. <https://doi.org/10.1016/j.jcis.2017.09.061>.
- Kathiravan, S., Jyothi, S., Ayyannan, G., Ravichandran, J., Raja, G., 2021. Inhibitory action of aqueous Ruellia Tuberosa L leaves extract on the corrosion of copper in HCl solution. *J. Indian Chem. Soc.* 98 (11), 100207. <https://doi.org/10.1016/j.jics.2021.100207>.
- Khalaf, M.M., Tantawy, A.H., Soliman, K.A., Abd El-Lateef, H.M., 2020. Cationic gemini-surfactants based on waste cooking oil as new 'green' inhibitors for N80-steel corrosion in sulphuric acid: a combined empirical and theoretical approaches. *J. Mol. Struct.* 1203, 127442. <https://doi.org/10.1016/j.molstruc.2019.127442>.
- Khan, G., Jeffrey, W., Newaz, S., Ahmed, P., Magaji, L., Muzamil, S., Mustafa, G., Abdur, M., Badarudin, A., Mohamad, B., 2017. Journal of colloid and interface science electrochemical investigation on the corrosion inhibition of mild steel by quinazolinone Schiff base compounds in hydrochloric acid solution. *J. Colloid Interface Sci.* 502, 134–145. <https://doi.org/10.1016/j.jcis.2017.04.061>.
- Khan, I., Ibrar, A., Abbas, N., Saeed, A., 2014. Recent advances in the structural library of functionalized quinazolinone and quinazolinone scaffolds: synthetic approaches and multifarious applications. *Eur. J. Med. Chem.* 76, 193–244. <https://doi.org/10.1016/j.ejmech.2014.02.005>.
- Kokalj, A., 2021. Molecular modeling of organic corrosion inhibitors: calculations, pitfalls, and conceptualization of molecule-surface bonding. *Corros. Sci.* 193, 109650. <https://doi.org/10.1016/J.CORSCI.2021.109650>.
- Kokalj, A., 2022. Corrosion inhibitors: physisorbed or chemisorbed? *Corros. Sci.* 196, 109939. <https://doi.org/10.1016/J.CORSCI.2021.109939>.
- Kumar, C. B. P., Prashanth, M. K., Mohana, K. N., Jagadeesha, M. B., Raghunath, M. S., Lokanath, N. K., and Kumar, K. Y. (2020). Protection of mild steel corrosion by three new quinazolinone derivatives : experimental and DFT studies. *Surf. Interfaces*, 18 (October 2019), 100446. Doi: 10.1016/j.surfint.2020.100446.
- Lgaz, H., Salghi, R., Jodeh, S., Hammouti, B., 2017. Effect of clozapine on inhibition of mild steel corrosion in 1.0 M HCl medium. *J. Mol. Liq.* 225, 271–280. <https://doi.org/10.1016/j.molliq.2016.11.039>.
- Lgaz, H., Masroor, S., Chafiq, M., Damej, M., Brahmia, A., Salghi, R., Benmessaoud, M., Ali, I.H., Alghamdi, M.M., Chaouiki, A., Chung, I.M., 2020. Evaluation of 2-mercaptobenzimidazole derivatives as corrosion inhibitors for mild steel in hydrochloric acid. *Metals* 10 (3), 1–14. <https://doi.org/10.3390/met10030357>.
- Lgaz, H., Chaouiki, A., Lamouri, R., Salghi, R., Lee, H.-S., 2021. Computational methods of corrosion inhibition assessment. In ACS Symposium Series. <https://doi.org/10.1021/bk-2021-1403.ch006>.
- Lgaz, H., Lee, H.S., 2022. First-principles based theoretical investigation of the adsorption of alkanethiols on the iron surface: a DFT-D3 study. *J. Mol. Liq.* 348, 118071. <https://doi.org/10.1016/j.molliq.2021.118071>.
- Li, W., Hu, L., Zhang, S., Hou, B., 2011. Effects of two fungicides on the corrosion resistance of copper in 3.5% NaCl solution under various conditions. *Corros. Sci.* 53 (2), 735–745. <https://doi.org/10.1016/j.corsci.2010.11.006>.
- Li, S.L., Wang, Y.G., Chen, S.H., Yu, R., Lei, S.B., Ma, H.Y., Liu, D.X., 1999. Some aspects of quantum chemical calculations for the study of Schiff base corrosion inhibitors on copper in NaCl solutions. *Corros. Sci.* 41 (9), 1769–1782. [https://doi.org/10.1016/S0010-938X\(99\)00014-1](https://doi.org/10.1016/S0010-938X(99)00014-1).
- Li, H., Zhang, S., Qiang, Y., 2021. Corrosion retardation effect of a green cauliflower extract on copper in H₂SO₄ solution: electrochemical and theoretical explorations. *J. Mol. Liq.* 321, 114450. <https://doi.org/10.1016/j.molliq.2020.114450>.
- Liao, Q.Q., Yue, Z.W., Yang, D., Wang, Z.H., Li, Z.H., Ge, H.H., Li, Y.J., 2011. Inhibition of copper corrosion in sodium chloride solution by the self-assembled monolayer of sodium diethyldithiocarbamate. *Corros. Sci.* 53 (5), 1999–2005. <https://doi.org/10.1016/j.corsci.2011.02.023>.
- Mammeri, S., Chafai, N., Harkat, H., Kerkour, R., Chafaa, S., 2021. Protection of steel against corrosion in acid medium using dihydropyrimidinone derivatives: experimental and DFT study. *Iran. J. Sci. Technol., Trans. A: Sci.* 45 (5), 1607–1619. <https://doi.org/10.1007/s40995-021-01140-1>.
- Medupin, R.O., Ukoba, K.O., Yoro, K.O., Jen, T.C., 2023. Sustainable approach for corrosion control in mild steel using plant-based inhibitors: a review. *Mater. Today Sustain.* 22, 100373. <https://doi.org/10.1016/J.MTSUST.2023.100373>.
- Moumeni, O., Chafaa, S., Kerkour, R., Benbouguerra, K., Chafai, N., 2020. Synthesis, structural and anticorrosion properties of diethyl (phenylamino) methyl phosphonate derivatives: experimental and theoretical study. *J. Mol. Struct.* 1206, 127693. <https://doi.org/10.1016/j.molstruc.2020.127693>.
- Mousavi, M., Bagholi, T., 2016. Application of interaction energy in quantitative structure-inhibition relationship study of some benzenethiol derivatives on copper corrosion. *Corros. Sci.* 105, 170–176. <https://doi.org/10.1016/j.corsci.2016.01.014>.
- Muralidharan, S., Puraishi, M.A., Iyer, S.V.K., 1995. The effect of molecular structure on hydrogen permeation and the corrosion inhibition of mild steel in acidic solutions. *Corros. Sci.* 37 (11), 1739–1750. [https://doi.org/10.1016/0010-938X\(95\)00668-U](https://doi.org/10.1016/0010-938X(95)00668-U).
- Noor, E.A., Al-Moubaraki, A.H., 2008. Thermodynamic study of metal corrosion and inhibitor adsorption processes in mild steel/1-methyl-4[(X)-styryl] pyridinium iodides/hydrochloric acid systems. *Mater. Chem. Phys.* 110 (1), 145–154. <https://doi.org/10.1016/J.MATCHEMP.2008.01.028>.
- Obot, I.B., Macdonald, D.D., Gasem, Z.M., 2015. Density functional theory (DFT) as a powerful tool for designing new organic corrosion inhibitors: part 1: an overview. *Corros. Sci.* 99, 1–30. <https://doi.org/10.1016/j.corsci.2015.01.037>.
- Obot, I.B., Haruna, K., Saleh, T.A., 2019. Atomistic simulation: a unique and powerful computational tool for corrosion inhibition research. *Arab. J. Sci. Eng.* 44 (1), 1–32. <https://doi.org/10.1007/s13369-018-3605-4>.
- Otmacic Kurkovic, H., Stupnisek-Lisac, E., Takenouti, H., 2010. The influence of pH value on the efficiency of imidazole based corrosion inhibitors of copper. *Corros. Sci.* 52 (2), 398–405. <https://doi.org/10.1016/j.corsci.2009.09.026>.
- Ouakki, M., Galai, M., Rbaa, M., Abousalem, A.S., Lakhri, B., Touhami, M.E., Cherkaoui, M., 2020. Electrochemical, thermodynamic and theoretical studies of some imidazole derivatives compounds as acid corrosion inhibitors for mild steel. *J. Mol. Liq.* 319, 114063. <https://doi.org/10.1016/j.molliq.2020.114063>.
- Oubaaq, M., Rbaa, M., Ouakki, M., Idouhli, R., Maatallah, M., Jarid, A., Warad, I., Abousalem, A.S., Lakhri, B., Zarrouk, A., Touhami, M.E., 2021. Novel triphenyl imidazole based on 8-hydroxyquinoline as corrosion inhibitor for mild steel in molar hydrochloric acid: experimental and theoretical investigations. *J. Appl. Electrochem.* 52, 413–433.
- Oubahou, M., Rbaa, M., Takky, D., Naimi, Y., Alrashdi, A.A., Lgaz, H., 2023. Elucidating the role of novel halogenated hydroquinazolinone derivatives in mitigating copper corrosion in saline conditions: a joint assessment of experimental outcomes and computational analysis. *J. Mol. Liq.* 390 (PA), 122966. <https://doi.org/10.1016/j.molliq.2023.122966>.
- Ouici, H.B., Benali, O., Harek, Y., Larabi, L., Hammouti, B., Guendouzi, A., 2013. Inhibition of mild steel corrosion in 5% HCl solution by 5-(2-hydroxyphenyl)-1,2,4-triazole-3-thione. *Res. Chem. Intermed.* 39 (6), 2777–2793. <https://doi.org/10.1007/s11664-012-0797-1>.

- Ouici, H.B., Benali, O., Guendouzi, A., 2015. Corrosion inhibition of mild steel in acidic media using newly synthesized heterocyclic organic molecules: correlation between inhibition efficiency and chemical structure. *AIP Conf. Proc.* 1653 <https://doi.org/10.1063/1.4914277>.
- Ouksel, L., Bourzami, R., Chafaa, S., Chafai, N., 2020. Solvent and catalyst-free synthesis, corrosion protection, thermodynamic, MDS and DFT calculation of two environmentally friendly inhibitors: bis-phosphonic acids. *J. Mol. Struct.* 1222, 128813 <https://doi.org/10.1016/j.molstruc.2020.128813>.
- Patel, M.B., Kumar, S.P., Valand, N.N., Jasrai, Y.T., Menon, S.K., 2013. Synthesis and biological evaluation of cationic fullerene quinazolinone conjugates and their binding mode with modeled mycobacterium tuberculosis hypoxanthine-guanine phosphoribosyltransferase enzyme. *J. Mol. Model.* 19 (8), 3201–3217. <https://doi.org/10.1007/s00894-013-1820-1>.
- Perdew, J.P., Burke, K., Ernzerhof, M., 1996. Generalized gradient approximation made simple. *Phys. Rev. Lett.* 77 (18), 3865–3868. <https://doi.org/10.1103/PhysRevLett.77.3865>.
- Rbaa, M., Lgaz, H., El Kacimi, Y., Lakhrissi, B., Bentiss, F., Zarrouk, A., 2018. Synthesis, characterization and corrosion inhibition studies of novel 8-hydroxyquinoline derivatives on the acidic corrosion of mild steel: experimental and computational studies. *Mater. Discover* 12 (August), 43–54. <https://doi.org/10.1016/j.md.2018.11.003>.
- Rbaa, M., Benhiba, F., Obot, I.B., Oudda, H., Warad, I., Lakhrissi, B., Zarrouk, A., 2019a. Two new 8-hydroxyquinoline derivatives as an efficient corrosion inhibitors for mild steel in hydrochloric acid: synthesis, electrochemical, surface morphological, UV-Visible and theoretical studies. *J. Mol. Liq.* 276, 120–133. <https://doi.org/10.1016/j.molliq.2018.11.104>.
- Rbaa, M., Galai, M., Benhiba, F., Obot, I.B., Oudda, H., Ebn Touhami, M., Lakhrissi, B., Zarrouk, A., 2019b. Synthesis and investigation of quinazolinone derivatives based on 8-hydroxyquinoline as corrosion inhibitors for mild steel in acidic environment: experimental and theoretical studies. *Ionics* 25 (7), 3473–3491. <https://doi.org/10.1007/s11581-018-2817-7>.
- Reddy, M.M., Sivaramakrishna, A., 2020. Remarkably flexible quinazolinones—synthesis and biological applications. *J. Heterocycl. Chem.* 57 (3), 942–954. <https://doi.org/10.1002/jhet.3844>.
- Rouifi, Z., Rbaa, M., Abousalem, A.S., Benhiba, F., Laabassi, T., Oudda, H., Lakhrissi, B., Guenbour, A., Warad, I., Zarrouk, A., 2020. Synthesis, characterization and corrosion inhibition potential of newly benzimidazole derivatives: combining theoretical and experimental study. *Surf. Interfaces* 18 (January). <https://doi.org/10.1016/j.surfint.2020.100442>.
- Saha, S.K., Murmu, M., Murmu, N.C., Banerjee, P., 2016. Evaluating electronic structure of quinazolinone and pyrimidinone molecules for its corrosion inhibition effectiveness on target species mild steel in the acidic medium: a combined DFT and MD simulation study. *J. Mol. Liq.* 224, 629–638. <https://doi.org/10.1016/j.molliq.2016.09.110>.
- Shaw, P., Obot, I.B., Yadav, M., 2019. Functionalized 2-hydrazinobenzothiazole with carbohydrates as a corrosion inhibitor: electrochemical, XPS, DFT and Monte Carlo simulation studies. *Mater. Chem. Front.* 3 (5), 931–940. <https://doi.org/10.1039/c9qm00096h>.
- Sherif, E.M., Erasmus, R.M., Comins, J.D., 2008. Inhibition of copper corrosion in acidic chloride pickling solutions by 5-(3-aminophenyl)-tetrazole as a corrosion inhibitor. *Corros. Sci.* 50 (12), 3439–3445. <https://doi.org/10.1016/j.corsci.2008.10.002>.
- Singh, R.P., Shukla, M.K., Mishra, A., Kumari, P., Reddy, C.R.K., Jha, B., 2011. Isolation and characterization of exopolysaccharides from seaweed associated bacteria *Bacillus licheniformis*. *Carbohydr. Polym.* 84 (3), 1019–1026. <https://doi.org/10.1016/j.carbpol.2010.12.061>.
- Soltani, N., Behpour, M., Ghoreishi, S.M., Naeimi, H., 2010. Corrosion inhibition of mild steel in hydrochloric acid solution by some double Schiff bases. *Corros. Sci.* 52 (4), 1351–1361. <https://doi.org/10.1016/j.corsci.2009.11.045>.
- Sukul, D., Pal, A., Mukhopadhyay, S., Saha, S.K., Banerjee, P., 2018. Electrochemical behaviour of uncoated and phosphatidylcholine coated copper in hydrochloric acid medium. *J. Mol. Liq.* 249, 930–940. <https://doi.org/10.1016/j.molliq.2017.11.129>.
- Sun, S., Geng, Y., Tian, L., Chen, S., Yan, Y., Hu, S., 2012. Density functional theory study of imidazole, benzimidazole and 2-mercaptobenzimidazole adsorption onto clean Cu (111) surface. *Corros. Sci.* 63, 140–147. <https://doi.org/10.1016/j.corsci.2012.05.024>.
- Sun, J., Wang, X., Gao, H., Chen, F., Wang, X., Zhang, J., Jin, Z., 2021. The effect of regional selectivity on the corrosion inhibition properties of synthetic ionic liquid via the synergistic action of the cation and anion. *New J. Chem.* 45 (43), 20201–20213. <https://doi.org/10.1039/D1NJ03529K>.
- Tait, W.S., 2018. Electrochemical corrosion basics. *Handbook of Environmental Degradation of Materials: Third Edition* 97–115. <https://doi.org/10.1016/B978-0-323-52472-8.00005-8>.
- Tan, B., Lan, W., Zhang, S., Deng, H., Qiang, Y., Fu, A., Ran, Y., Xiong, J., Marzouki, R., Li, W., 2022a. *Passiflora edulis* Sims leaves extract as renewable and degradable inhibitor for copper in sulfuric acid solution. *Colloids Surf. A: Physicochem. Eng. Aspects* 645 (February), 128892. <https://doi.org/10.1016/j.colsurfa.2022.128892>.
- Tan, B., Zhang, S., Cao, X., Fu, A., Guo, L., Marzouki, R., Li, W., 2022b. Insight into the anti-corrosion performance of two food flavors as eco-friendly and ultra-high performance inhibitors for copper in sulfuric acid medium. *J. Colloid Interface Sci.* 609, 838–851. <https://doi.org/10.1016/j.jcis.2021.11.085>.
- Tan, B., Fu, A., Guo, L., Ran, Y., Xiong, J., Marzouki, R., Li, W., 2023a. Insight into anti-corrosion mechanism of *Dalbergia odorifera* leaves extract as a biodegradable inhibitor for X70 steel in sulfuric acid medium. *Ind. Crop. Prod.* 194 (December 2022), 116106 <https://doi.org/10.1016/j.indcrop.2022.116106>.
- Tan, L., Li, J., Zeng, X., 2023b. Revealing the correlation between molecular structure and corrosion inhibition characteristics of N-heterocycles in terms of substituent groups. *Materials* 16 (6), 2148. <https://doi.org/10.3390/ma16062148>.
- Tang, J., Hu, Y., Han, Z., Wang, H., Zhu, Y., Wang, Y., Nie, Z., Wang, Y., 2018. Experimental and theoretical study on the synergistic inhibition effect of pyridine derivatives and sulfur-containing compounds on the corrosion of carbon steel in CO₂-saturated 3.5 wt.% NaCl solution. *Molecules* 23 (12). <https://doi.org/10.3390/molecules23123270>.
- Tantawy, A.H., Soliman, K.A., Abd El-Lateef, H.M., 2021. Experimental and computational approaches of sustainable quaternary bisammonium fluorosurfactants for corrosion inhibition as protective films at mild steel/H₂SO₄ interface. *Colloids Surf. A Physicochem. Eng. Asp.* 614 (October 2020), 126141 <https://doi.org/10.1016/j.colsurfa.2021.126141>.
- Tasić, Ž.Z., Petrović Mihajlović, M.B., Radovanović, M.B., Simonović, A.T., Antonijević, M.M., 2021. Experimental and theoretical studies of paracetamol as a copper corrosion inhibitor. *J. Mol. Liq.* 327 <https://doi.org/10.1016/j.molliq.2020.114817>.
- Thomas K.V., Thomas K.J., Rapheal P.V., Sabu, A.S., Ragi, K., Johnson, R. (2021). *Tinospora cordifolia* extract as an environmentally benign green corrosion inhibitor in acid media: electrochemical, surface morphological, quantum chemical, and statistical investigations. *Mater. Today Sustain.*, 13, 100076. Doi: 10.1016/J.MTSUST.2021.100076.
- Tribollet, B., 1994. Anodic dissolution of metal coated by a formed salt film. In: Trethewey, K.R., Roberge, P.R. (Eds.), *Modelling Aqueous Corrosion: from Individual Pits to System Management*. Springer, Netherlands, pp. 141–159. https://doi.org/10.1007/978-94-011-1176-8_7.
- Umoren, S.A., Solomon, M.M., Saji, V.S., 2022. Mechanism of corrosion inhibition by polymers. *Polym. Mater. Corrosion Inhibition* 565–589. <https://doi.org/10.1016/B978-0-12-823854-7.00005-9>.
- Verma, C., Ebenso, E.E., Quraishi, M.A., 2017. Corrosion inhibitors for ferrous and non-ferrous metals and alloys in ionic sodium chloride solutions: a review. *J. Mol. Liq.* 248, 927–942. <https://doi.org/10.1016/j.molliq.2017.10.094>.
- Verma, C., Olasunkanmi, L.O., Ebenso, E.E., Quraishi, M.A., 2018a. Substituents effect on corrosion inhibition performance of organic compounds in aggressive ionic solutions: a review. *J. Mol. Liq.* 251, 100–118. <https://doi.org/10.1016/j.molliq.2017.12.055>.
- Verma, C., Quraishi, M.A., Ebenso, E.E., Bahadur, I., 2018b. A green and sustainable approach for mild steel acidic corrosion inhibition using leaves extract: experimental and DFT studies. *J. Bio- and Tribo-Corrosion* 4 (3). <https://doi.org/10.1007/s40735-018-0150-3>.
- Verma, C., Quraishi, M.A., Lgaz, H., Olasunkanmi, L.O., Sherif, E.S.M., Salghi, R., Ebenso, E.E., 2019. Adsorption and anticorrosion behaviour of mild steel treated with 2-((1H-indol-2-yl)thio)-6-amino-4-phenylpyridine-3,5-dicarbonitriles in a hydrochloric acid solution: experimental and computational studies. *J. Mol. Liq.* 283, 491–506. <https://doi.org/10.1016/j.molliq.2019.03.105>.
- Verma, C., Quraishi, M.A., Ebenso, E.E., 2020. Quinoline and its derivatives as corrosion inhibitors: a review. *Surf. Interfaces* 21 (June). <https://doi.org/10.1016/j.surfint.2020.100634>.
- Vitos, L., Ruban, A.V., Skriver, H.L., Kollár, J., 1998. The surface energy of metals. *Surf. Sci.* 411 (1–2), 186–202. [https://doi.org/10.1016/S0039-6028\(98\)00363-X](https://doi.org/10.1016/S0039-6028(98)00363-X).
- Walczak, M.S., Morales-Gil, P., Lindsay, R., 2019. Determining Gibbs energies of adsorption from corrosion inhibition efficiencies: is it a reliable approach? *Corros. Sci.* 155 (May), 182–185. <https://doi.org/10.1016/j.corsci.2019.04.040>.
- Wei, H., Heidarshenas, B., Zhou, L., Hussain, G., Li, Q., & Ostrikov, K. (Ken). (2020). Green inhibitors for steel corrosion in acidic environment: state of art. *Mater. Today Sustain.*, 10, 100044. Doi: 10.1016/J.MTSUST.2020.100044.
- White, P.A., Collis, G.E., Skidmore, M., Breedon, M., Ganther, W.D., Venkatesan, K., 2020. Towards materials discovery: assays for screening and study of chemical interactions of novel corrosion inhibitors in solution and coatings. *New J. Chem.* 44 (19), 7647–7658. <https://doi.org/10.1039/C9NJ06456G>.
- Xia, T., Zeng, L., Zhang, X., Liu, J., Zhang, W., Liang, T., Yang, B., 2019. Enhanced corrosion resistance of a Cu–10Ni alloy in a 3.5 wt% NaCl solution by means of ultrasonic surface rolling treatment. *Surf. Coat. Technol.* 363 (November 2018), 390–399. <https://doi.org/10.1016/j.surfcoat.2019.02.039>.
- Yadav, D.K., Quraishi, M.A., 2012. Application of some condensed uracils as corrosion inhibitors for mild steel: gravimetric, electrochemical, surface morphological, UV-visible, and theoretical investigations. *Ind. Eng. Chem. Res.* 51 (46), 14966–14979. <https://doi.org/10.1021/ie301840y>.
- Yao, X., Lai, Y., Huang, F., Qiang, Y., Jin, Y., 2021. 5,5'-dithiobis(2-nitrobenzoic acid) self-assembled monolayer for corrosion inhibition of copper in sodium chloride solution. *J. Mol. Liq.* 343, 117535 <https://doi.org/10.1016/j.molliq.2021.117535>.
- Yildiz, R., Döner, A., Doğan, T., Dehri, I., 2014. Experimental studies of 2-pyridinecarboxitrile as corrosion inhibitor for mild steel in hydrochloric acid solution. *Corros. Sci.* 82, 125–132. <https://doi.org/10.1016/j.corsci.2014.01.008>.
- Zaafarany, I., 2009. Phenyl phthalimide as corrosion inhibitor for corrosion of C-steel in sulphuric acid solution. *Port. Electrochim. Acta* 27 (5), 631–643. <https://doi.org/10.4152/pea.200905631>.
- Zhang, H.H., Chen, Y., Zhang, Z., 2018a. Comparative studies of two benzaldehyde thiosemicarbazone derivatives as corrosion inhibitors for mild steel in 1.0 M HCl. *Results Phys.* 11 (September), 554–563. <https://doi.org/10.1016/j.rinp.2018.09.038>.
- Zhang, W., Ma, R., Liu, H., Liu, Y., Li, S., Niu, L., 2016. Electrochemical and surface analysis studies of 2-(quinolin-2-yl)quinazolin-4(3H)-one as corrosion inhibitor for Q235 steel in hydrochloric acid. *J. Mol. Liq.* 222, 671–679. <https://doi.org/10.1016/j.molliq.2016.07.119>.

Zhang, W., Li, H.-J., Wang, Y., Liu, Y., Gu, Q.-Z., Wu, Y.-C., 2018b. Gravimetric, electrochemical and surface studies on the anticorrosive properties of 1-(2-pyridyl)-2-thiourea and 2-(imidazol-2-yl)-pyridine for mild steel in hydrochloric acid. *New J. Chem.* 42 (15), 12649–12665. <https://doi.org/10.1039/C8NJ01762J>.

Zhang, W., Li, H.J., Wang, M., Wang, L.J., Shang, F., Wu, Y.C., 2018c. Halogen-substituted acridines as highly effective corrosion inhibitors for mild steel in acid

medium. *J. Phys. Chem. C* 122 (44), 25349–25364. <https://doi.org/10.1021/acs.jpcc.8b07015>.

Zhang, J., Zhang, S., 2021. Study of novel quinazolinone derivatives with different chain lengths as corrosion inhibitors for copper in 0.5 M sulfuric acid medium. *Int. J. Electrochem. Sci.* 16 (7), 1–17. <https://doi.org/10.20964/2021.07.11>.